ACS OMEGA

http://pubs.acs.org/journal/acsodf

Article

Improving the Solubility of Hexanuclear Heterometallic Extended Metal Atom Chain Compounds in Nonpolar Solvents by Introducing Alkyl Amine Moieties

Kazuhiro Uemura,* Erina Yasuda, and Yuko Sugiyama

Cite This: *ACS Omega* 2021, 6, 18487−18503

Read Online

ACCESS | Metrics & More | Article Recommendations | Supporting Information

ABSTRACT: The highest occupied molecular orbital−lowest unoccupied molecular orbital (HOMO−LUMO) interaction at the d_{z^2} orbital between two kinds of metal complex is useful for obtaining heterometallic one-dimensional (1D) chains as well as heterometallic metal string compounds (HMSCs). Platinum dinuclear complexes, $[Pt_2(piam)_2(NH_2R)_4]X_2$ (piam = pivalamidate, R = CH_3, C_2H_5, C_3H_7, or C_4H_9, X = anion), comprising σ^* as HOMO were mixed with $[Rh_2(O_2CCH_3)_4]$ comprising σ^* as LUMO in solvents to afford single crystals of $[\{Rh_2(O_2CCH_3)_4\}\{Pt_2(piam)_2(NH_2R)_4\}_2]X_4$ (**2**−**5**). Single-crystal X-ray analyses revealed that **2**−**5** are hexanuclear complexes that are one-dimensionally aligned as Pt−Pt−Rh−Rh−Pt−Pt with metal−metal bonds, where the alkyl moieties at end Pt atoms obstruct further 1D extension. Complexes **2**−**5** appear as if they are cut off from an infinite chain $[\{Rh_2(O_2CCH_3)_4\}\{Pt_2(piam)_2(NH_3)_4\}_2]_n(PF_6)_{4n}\cdot 6nH_2O$ (**1**) aligned as $-\{Pt-Pt-Rh-Rh-Pt-Pt\}_n-$. The diffuse reflectance spectrum of **1** depicts broad shoulder bands, which are not present in the spectra of **2**−**5**, proving that the infinite chain **1** forms a band structure. Compounds **4** and **5** with propyl or butyl moieties at amine ligands, respectively, are soluble in nonpolar solvents, such as CH_2Cl_2, without the dissociation of their hexanuclear structures. Taking advantage of their solubility, measurement of cyclic voltammetry in CH_2Cl_2 become possible, which shows the quasi-reversible oxidation and reduction waves at **4**: E_{ox} = 0.86 V and E_{red} = 0.69 V and **5**: E_{ox} = 0.87 V and E_{red} = 0.53 V.

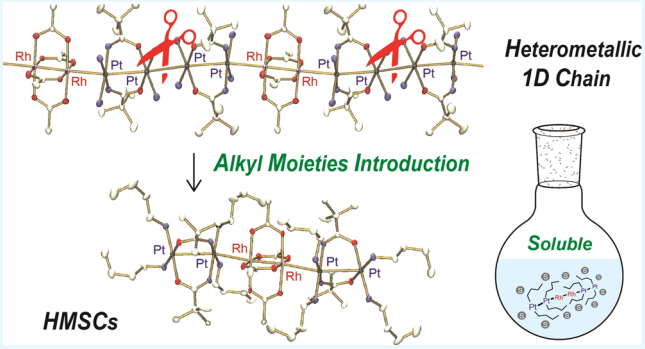

INTRODUCTION

The exploration of a useful synthetic method for manufacturing one-dimensional (1D) metal wires is still sustained by their advantageous physical properties of high anisotropy,[1−5] because 1D metal wires containing element block are used in various applications, such as light-emitting diodes, photovoltaic cells, and molecular sensors.[6−8] Extended metal atom chains (EMACs), where metals are one-dimensionally arranged by metal−metal bonds, are advantageous as various electronic structures can be obtained by tuning the metal species and their oxidation states.[9−24] The major synthetic approach for EMACs is the template method, where the metals are reacted with preprogramed ligands, such as oligopyridylamine,[9−17] oligophosphine,[18−21] and π-conjugated ligand,[22−24] to align metals with metal−metal bonds by controlling the number of metal atoms by the length of the organic ligand. Recently, heterometallic EMAC compounds (HEMACs), also known as heterometallic metal string compounds (HMSCs),[25,26] have been synthesized, where a few kinds of metal species are regularly aligned; for example, $M_A-M_A-M_B$,[27−44] Ni−Ru−Ru−Ni−Ni,[45] and Ni−Ni−Ru−Ru−Ni−Ni−Ni,[46] with two kinds of metal species; $M_A-M_B-M_C$, with three kinds of metal species;[47,48] and surprisingly Ni−Pt−Co−Co−Pd, with four kinds of metal species[49] were realized with a molecular rectifier[45] and large ferromagnetic coupling thorough metal−metal bonds.[42] To align metals by regulating number and species at will, rational and systematic synthesis methods are currently being explored.

In previous study, we synthesized heterometallic 1D chains using the highest occupied molecular orbital−lowest unoccupied molecular orbital (HOMO−LUMO) interaction in the σ^* (d_{z^2}) orbital between two kinds of metal complexes.[50] For example, platinum dinuclear complex $[Pt_2(piam)_2(NH_3)_4](PF_6)_2$ (piam = pivalamidate) and rhodium dinuclear complex $[Rh_2(O_2CCH_3)_4]$ with HOMO and LUMO in σ^*, respectively, were mixed in an adequate solvent to yield the crystals for $[\{Rh_2(O_2CCH_3)_4\}\{Pt_2(piam)_2(NH_3)_4\}_2]_n(PF_6)_{4n}\cdot 6nH_2O$ (**1**), which contains 1D chains aligned as $-\{Pt-Pt-Rh-Rh-Pt-$

Received: May 19, 2021
Accepted: June 24, 2021
Published: July 7, 2021

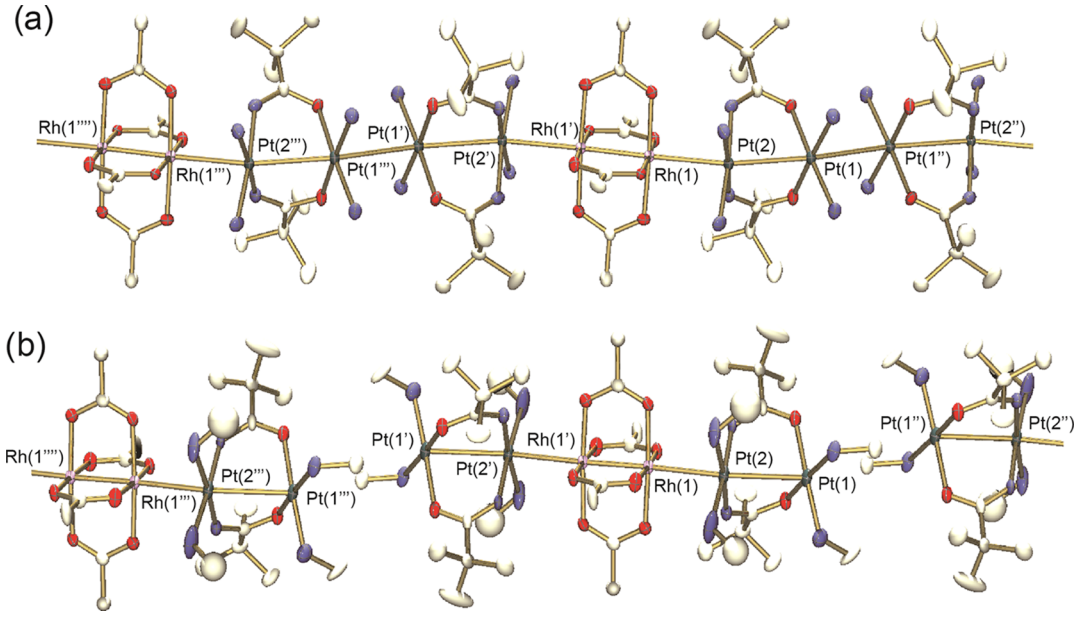

Figure 1. Crystal structures of (a) $[\{Rh_2(O_2CCH_3)_4\}\{Pt_2(piam)_2(NH_3)_4\}_2]_n(PF_6)_{4n}\cdot 6nH_2O$ (**1**) and (b) $[\{Rh_2(O_2CCH_3)_4\}\{Pt_2(piam)_2(NH_2CH_3)_4\}_2](PF_6)_4$ (**2**).

Scheme 1. Heterometallic 1D Chains Constructed by HOMO−LUMO Interaction at d_{z^2} Orbitals with Variable Metal Alignments

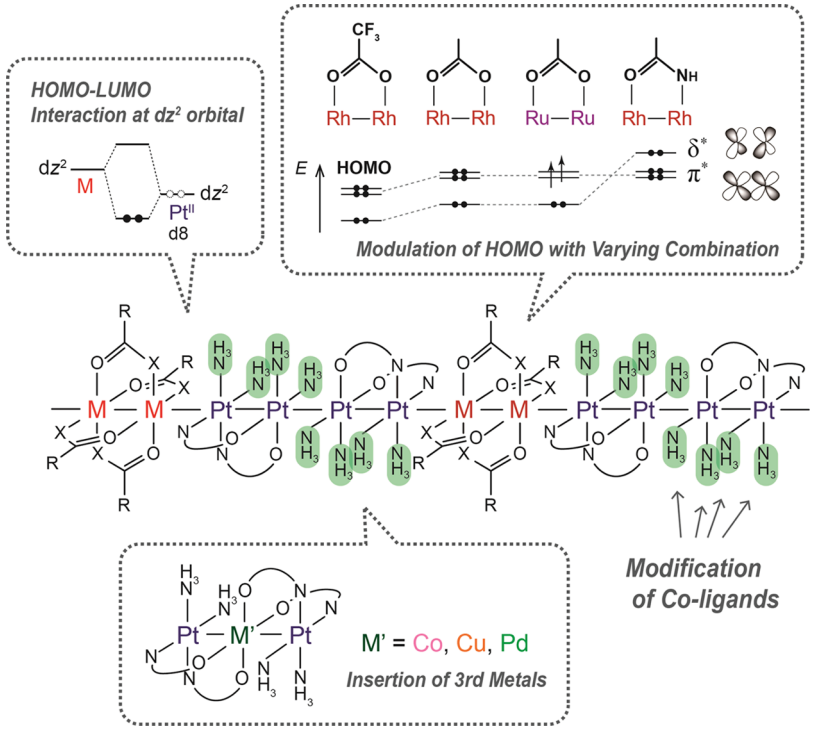

Pt}$_n$− (Figure 1a).[51] Interestingly, this synthetic method is versatile: various 1D chains modulated in electronic structures can be attained by selecting the metal species and bridging ligands in dinuclear LUMO parts[52−54] or trinuclear complex Pt−M−Pt in HOMO parts;[54−56] thus, band gap modulation[54] and paramagnetism[53,55−57] are achieved through metal−metal bonds (Scheme 1).

In this study, we applied this rational metal extension method for infinite 1D chains, the HOMO−LUMO interaction in σ^* (d_{z^2}) orbital, to synthesize HMSCs. As shown in Figure 1a, the unbridged Pt−Rh bonds in **1** are formed by not only HOMO−LUMO interactions in σ^* but also quadruple hydrogen bonds between Pt-coordinated NH_3 or NH (piam) and Rh-coordinated O atoms. The ligands coordinated to the end Pt atoms are also quadruple hydrogen-bonded, and thus, they support the formation of end Pt−Pt bonds as infinite −{Pt−Pt−Rh−Rh−Pt−Pt}$_n$− chains.[51] In contrast, when a dinuclear platinum complex has different co-ligands, such as NH_2CH_3 from NH_3, a hexanuclear complex $[\{Rh_2(O_2CCH_3)_4\}\{Pt_2(piam)_2(NH_2CH_3)_4\}_2](PF_6)_4$ (**2**) aligned as Pt−Pt−Rh−Rh−Pt−Pt is afforded (Figure 1b), where end Pt−Pt bonds are not formed despite the formation of unbridged Pt−Rh bonds.[58]

https://doi.org/10.1021/acsomega.1c02634
ACS Omega 2021, 6, 18487−18503

These results indicate that the unbridged Pt−Rh bond in this system is relatively strong, but the end Pt−Pt bond is not formed without the support of hydrogen bonds. Using these findings, novel hexanuclear HMSCs containing two unbridged Pt−Rh bonds were designed by introducing alkyl moieties in co-ligands in Pt atoms. In this study, the syntheses, structures, and physical properties of three hexanuclear HMSCs with $NH_2C_2H_5$, $NH_2C_3H_7$, or $NH_2C_4H_9$ in co-ligands in Pt atoms are shown. Fortunately, the hexanuclear complexes comprising $NH_2C_3H_7$ or $NH_2C_4H_9$ are improved with solubility in nonpolar solvents without the collapse of their hexanuclear backbones. The electronic structures, solubilities, and redox behaviors are discussed by comparing several physical measurements and calculations.

RESULTS AND DISCUSSION

Synthetic Procedure. To rationally introduce alkyl moieties at amines coordinated to Pt atoms in the 1D heterometallic complexes, amidate-hanging platinum mononuclear complexes *cis*-$[Pt(piam)_2(NH_2CH_3)_2]\cdot H_2O$,[59] *cis*-$[Pt(piam)_2(NH_2C_2H_5)_2]\cdot H_2O$,[60] *cis*-$[Pt(piam)_2(NH_2C_3H_7)_2]\cdot H_2O$,[61] and *cis*-$[Pt(piam)_2(NH_2C_4H_9)_2]$[61] were used. These complexes were easily dimerized with aqua Pt complexes having corresponding alkyl amines, *cis*-$[Pt(OH_2)_2(NH_2R)_2]$ (R = CH_3, C_2H_5, C_3H_7 and C_4H_9), to provide dinuclear platinum complexes, $[Pt_2(piam)_2(NH_2R)_4]X_2$ (X = anion). Similar to previous synthetic procedures[58] (Scheme 2), novel heterometallic complexes were successfully obtained, $[\{Rh_2(O_2CCH_3)_4\}\{Pt_2(piam)_2(NH_2C_2H_5)_4\}_2](PF_6)_4$ (**3**), $[\{Rh_2(O_2CCH_3)_4\}\{Pt_2(piam)_2(NH_2C_3H_7)_4\}_2](PF_6)_3(ClO_4)$ (**4**), and $[\{Rh_2(O_2CCH_3)_4\}\{Pt_2(piam)_2(NH_2C_4H_9)_4\}_2](ClO_4)_4$ (**5**), by selecting adequate counter anions and solvents.

Scheme 2. Synthetic Route for Heterometallic 1D Hexanuclear Complexes 1−5

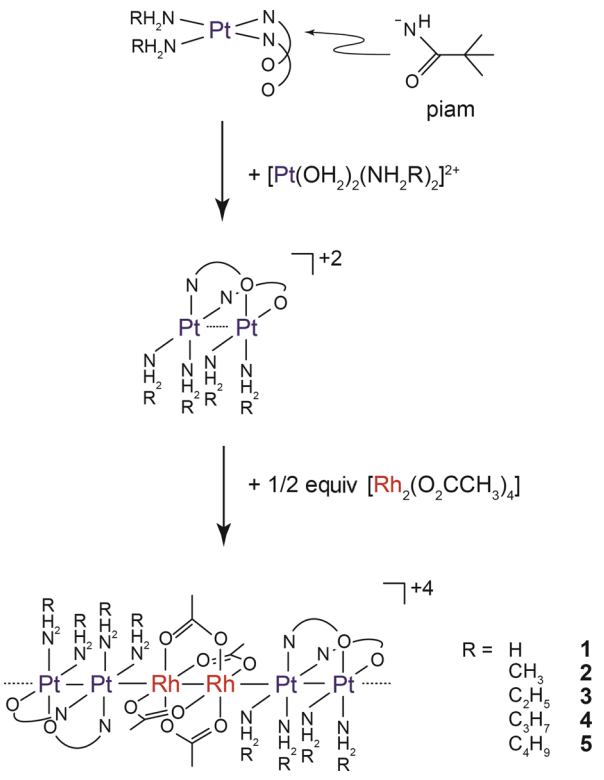

Crystal Structures and Oxidation States of 3−5. Figure 2 shows the crystal structure of **3**. The dinuclear paddle wheel complexes of $[Rh_2(O_2CCH_3)_4]$ are sandwiched by $[Pt_2(piam)_2(NH_2C_2H_5)_4]$ at both ends with metal−metal bonds to form [Pt−Pt]−[Rh−Rh]−[Pt−Pt] units, where a crystallographic inversion center lies at the center of the rhodium complex (Figure 2a). These hexanuclear units in **3** are similar to those in **2**. Three kinds of angles are defined here as that θ is the angle through metal−metal bonds; ϕ is the twist angles between the coordination plane; and τ is the dihedral angles of coordination planes (Scheme 3). The platinum dinuclear complexes are bonded to a rhodium complex with a bond distance of Pt(2)−Rh(1) = 2.8321(5) Å and a torsion angle N−Pt−Rh−O (ϕ_2) of about 16−23° (Figure 2b). Between [Pt−Pt] and [Rh−Rh], the ethyl groups of $NH_2C_2H_5$ are tilted toward [Pt−Pt], which permits multiple hydrogen bonds between the nitrogen atoms of the amine/amidate ligands in [Pt−Pt] and the carboxylate oxygen atoms in [Rh−Rh] with N−O bond distances of 2.9−3.0 Å. The dihedral angle (τ_2) between the RhO_4 and PtN_4 planes is small (2.6°), indicating that the Rh and Pt planes are arranged in a face-to-face fashion. The τ_3 between the two Pt coordination planes is relatively large (37°), which is caused by the half-lantern fashion of the piam bridges. The average torsional twist angle (ϕ_3) about the Pt−Pt axis within the [Pt−Pt] is 7.5°. In the entire crystal, each hexanuclear [Pt−Pt]−[Rh−Rh]−[Pt−Pt] unit is packed in parallel (Figure 2c), where the methyl groups of $NH_2C_2H_5$ on terminal platinum atoms obstruct the close contact to the neighboring hexanuclear unit (Pt−Pt = 5.59 Å), resulting in no formation of infinite 1D chains.

Figures 3 and 4 show the crystal structures of $[\{Rh_2(O_2CCH_3)_4\}\{Pt_2(piam)_2(NH_2C_3H_7)_4\}_2](PF_6)_3(ClO_4)$ (**4**) and $[\{Rh_2(O_2CCH_3)_4\}\{Pt_2(piam)_2(NH_2C_4H_9)_4\}_2](ClO_4)_4$ (**5**), respectively. Each compound also forms hexanuclear complexes expressed as [Pt−Pt]−[Rh−Rh]−[Pt−Pt] (Figures 3a and 4a). The alkyl moieties at amine ligands coordinated to inner Pt atoms protrude along the coordination planes, where effective hydrogen bonds are formed between inner Pt and Rh coordination planes. The Pt−Rh distances are 2.7536(6) Å (**4**) and 2.8030(11) Å (**5**), where [Pt−Pt] and [Rh−Rh] are stacked in a staggered fashion with torsion angles N−Pt−Rh−O (ϕ_2) of approximately 35−39° (**4**) and 31−34° (**5**). The end methyl groups at inner alkyl moieties are closer to $^-O_2CCH_3$ ligands, as if surrounding the [Rh−Rh] parts. On the contrary, outer alkyl moieties at amine ligands coordinated to outer Pt atoms protrude along the metal−metal bonds, affording greater differences between hexanuclear complexes with longer alkyl moieties, where the distances between end platinum atoms of outer Pt and neighboring ones are 5.54 Å (**4**) and 10.66 Å (**5**). In **4**, the determination of the position of ClO_4^- ions in the crystal is difficult due to the high disorder; however, the results of elemental analysis and electrospray ionization mass spectrometry (ESI-MS) spectra revealed that the formula of **4** is $[\{Rh_2(O_2CCH_3)_4\}\{Pt_2(piam)_2(NH_2C_3H_7)_4\}_2](PF_6)_3(ClO_4)$.

Table 1 summarizes metal−metal distances and angles for **1**−**5**. The values of θ, ϕ, and τ are almost similar. The ϕ_2 values between [Pt−Pt] and [Rh−Rh] are in the range of 20−43°, showing twist fashion. No trend in Rh−Pt distances exists depending on the length of alkyl moieties. In **1**−**5**, the Pt−Pt distances are 2.94−3.02 Å, which are typical for Pt(+2)−Pt(+2) oxidation states.[62]

https://doi.org/10.1021/acsomega.1c02634
ACS Omega 2021, 6, 18487−18503

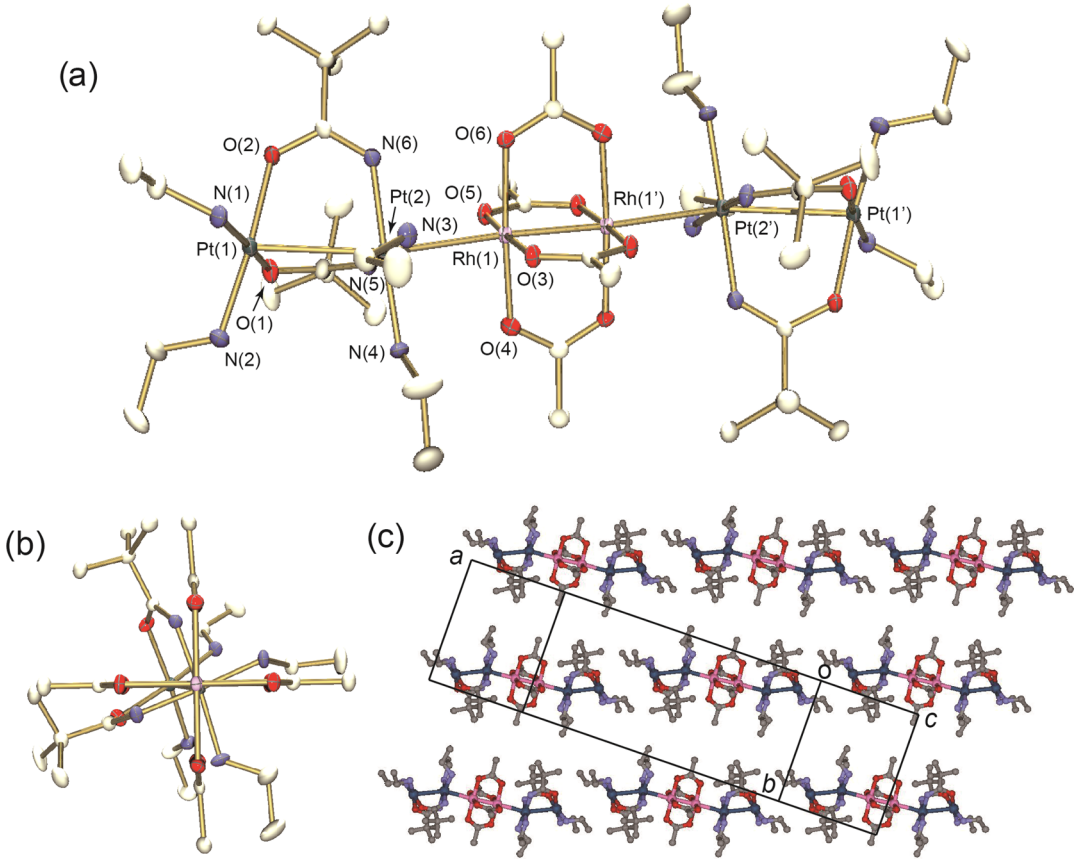

Figure 2. (a) Crystal structure of $[\{Rh_2(O_2CCH_3)_4\}\{Pt_2(piam)_2(NH_2C_2H_5)_4\}_2](PF_6)_4$ (**3**). (b) Stacking fashion between rhodium dinuclear complex and platinum dinuclear complex in **3**. (c) Packing view of **3**. The hydrogen atoms and anions are omitted for clarity.

Scheme 3. Angles (θ) through Metal−Metal Bonds, Torsional Twist Angles (ϕ), and Dihedral Angles (τ) in Heterometallic Hexanuclear Complexes

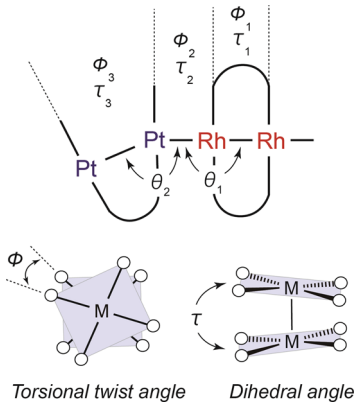

Several hexanuclear EMACs bridged by polyphenylphosphine or polypyridyl amine ligands,[63−68] such as $[Pt_6(\mu\text{-dpmp})_4(XylNC)_2](PF_6)_4$ (dpmp = bis-(diphenylphosphanylmethyl)phenylphosphane, Xyl = 2,6-dimethylphenyl),[63] $[Co_6(\mu_6\text{-bpyany})_4(NCS)_2]PF_6$ (H_2bpyany = 2,7-bis(α-pyridylamino)-1,8-naphthyridine),[64] and $[Ni_6(\mu_6\text{-bpmany})_4(NCS)_2]Cl$ (H_2bpmany = 2,7-bis(α-pyrimidylamino)-1,8-naphthyridine),[66] have been reported. Compared to these EMACs, the characteristic features for **2**−**5** contain two unbridged metal−metal (Pt−Rh) bonds, which are similar to those for the previous hexanuclear compound HH,HT,HH-$[Ir_6(\mu\text{-OPy})_6(I)_2(CO)_{12}]$ (Opy = 2-pyridonate), which comprises three dinuclear Ir complexes aligned as Ir−Ir−Ir−Ir−Ir−Ir.[69,70] In HH,HT,HH-$[Ir_6(\mu\text{-OPy})_6(I)_2(CO)_{12}]$, six iridium atoms have a formal oxidation state of +1.33, where the sum of oxidation state is +8, indicating that 46 d-electrons are present over six iridium atoms. Moreover, in **2**−**5**, the formulas based on the crystal structures and elemental analyses revealed that the sum of the metal oxidation state of hexanuclear Pt−Pt−Rh−Rh−Pt−Pt is +12, which indicates 46 d-electrons in four Pt and two Rh atoms. Considering that the Pt−Pt distances in the crystal structures revealed typical d^8−d^8 configurations, Rh−Rh comprised d^7−d^7 configurations and resulted in the formal oxidation state of Pt(+2)−Pt(+2)−Rh(+2)−Rh(+2)−Pt(+2)−Pt(+2), which were not changed from the original compounds. This oxidation state is similar to that in the prototype 1D chain **1**. To further estimate the oxidation states, X-ray photoelectron spectroscopy (XPS) measurements were performed (Figure S5). The XPS spectra of **2**−**5** in the Rh 3d and Pt 4f regions at room temperature show that the Rh $3d_{5/2}$ binding energy values are 308.6 (**2**), 308.8 (**3**), 308.7 (**4**), and 308.8 (**5**) eV. In addition, the Pt $4f_{7/2}$ binding energy values are 73.1 (**2**), 73.2 (**3**), 72.9 (**4**), and 73.0 (**5**) eV. These values well coincide with those in **1**, supporting the Pt(+2)−Pt(+2)−Rh(+2)−Rh(+2)−Pt(+2)−Pt(+2) oxidation state.

Compounds **2**−**5** are considered as if they are cut from the 1D chain **1** as hexanuclear units, because the metal repetition, metal−metal distances, and oxidation states are similar. In other previous metal complexes introducing alkyl moieties in coordinated ligands,[71−73] the hydrophobic interaction among side ligands induces the aggregation of metal cores, thus affording the infinite 1D chains. Furthermore, in **2**−**5**, outer

https://doi.org/10.1021/acsomega.1c02634
ACS Omega 2021, 6, 18487−18503

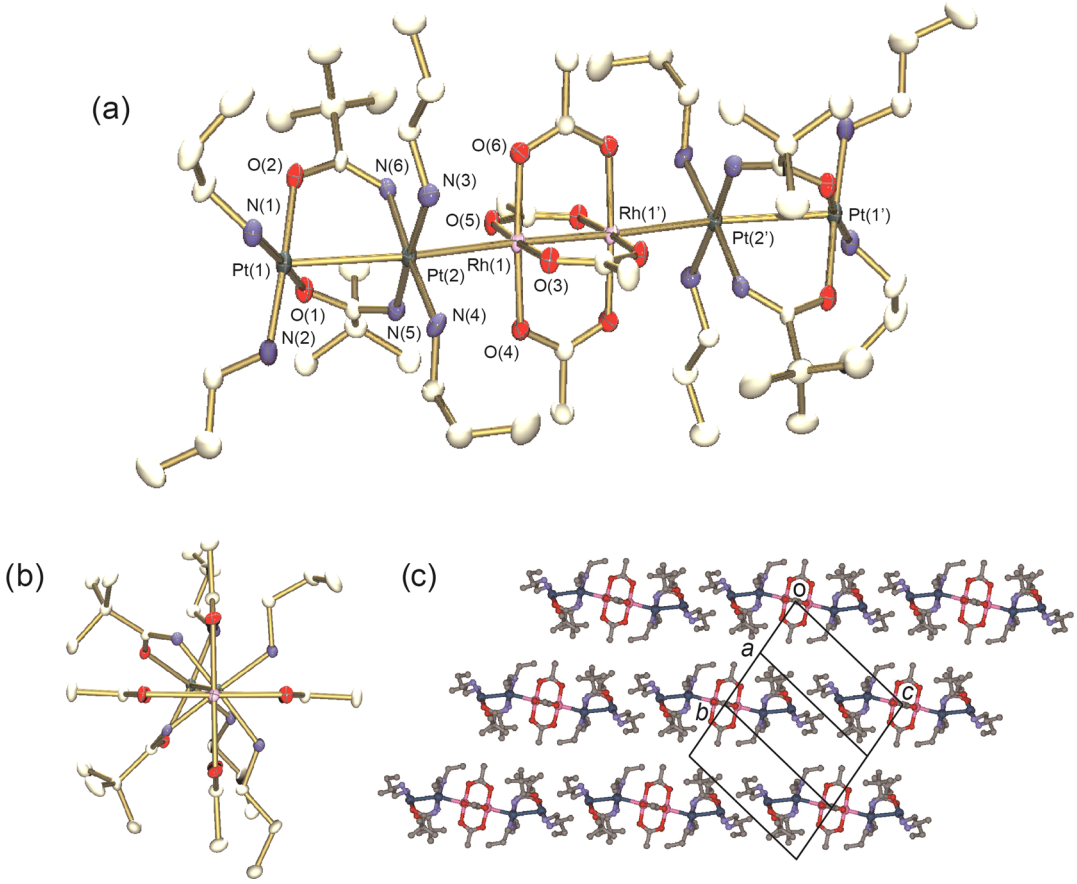

Figure 3. (a) Crystal structure of $[\{Rh_2(O_2CCH_3)_4\}\{Pt_2(piam)_2(NH_2C_3H_7)_4\}_2](PF_6)_3(ClO_4)$ (**4**). (b) Stacking fashion between rhodium dinuclear complex and platinum dinuclear complex in **4**. (c) Packing view of **4**. The hydrogen atoms and anions are omitted for clarity.

alkyl moieties obstruct the further extension to become HMSCs. The Pt−Rh bonds afforded by the HOMO−LUMO interaction along the *z* axis overcome the obstruction of inner alkyl moieties, indicating that these heterometallic bonds are relatively strong, but the unbridged Pt−Pt bonds found in **1** are relatively weak. This system was successful in cutting the hexanuclear units from **1** by introducing alkyl moieties at the co-ligands.

Electronic Structures and Absorption Spectra. Figures 5−7 and S6−S33 show the results of density functional theory (DFT) calculations of the model of $[\{Rh_2(O_2CCH_3)_4\}\{Pt_2(NHCOR')_2(NH_2R)_4\}_2]^{4+}$ (R = CH_3, C_2H_5, C_3H_7 or C_4H_9; R′ = CH_3 or ^{t}Bu) based on the crystal structures. Based on the crystal structures of **2**−**5**, the model structures $[\{Rh_2(O_2CCH_3)_4\}\{Pt_2(NHCOCH_3)_2(NH_2R)_4\}_2]^{4+}$ were calculated to obtain optimized structures **na** (n = 2, R = CH_3; n = 3, R = C_2H_5; n = 4, R = C_3H_7; n = 5, R = C_4H_9), **nb** under the rigid condition of metal coordinates, and **nc** under the rigid condition of metal and coordinated atom coordinates. Furthermore, the model structures $[\{Rh_2(O_2CCH_3)_4\}\{Pt_2(NHCO^tBu)_2(NH_2R)_4\}_2]^{4+}$ were calculated to obtain optimized structures **nd**, structures **ne** under the rigid condition of metal coordinates, and structures **nf** under the rigid condition of metal and coordinated atom coordinates. Thus, for **2**−**5**, six optimized structures **na**−**nf** were obtained, respectively. As shown in Figures S6−S33, comparing **na**−**nc** and **nd**−**nf**, cardinal electronic structures do not depend on whether CH_3 or ^{t}Bu is present at the bridging ligands of Pt dinuclear complexes; this indicates that the ligands of $^-$NHCOR′ do not significantly influence the electronic structures of **2**−**5**. Figure 5 shows optimized structures and shapes of LUMO and HOMO for **2a**−**c**. In the optimized structure of **2a**, the metal−metal distances are longer than those in the crystal structure of **2** (Table S1), where the Pt−Pt distance is 3.55 Å and shows no significant metal−metal interactions. Moreover, the twist angle (ϕ_2) between [Rh−Rh] and [Pt−Pt] is 5.6°, as it is close to face-to-face stacking. In contrast, in **2b** and **2c**, the values of twist angle ϕ_2 calculated under rigid conditions are closer to the crystal structure. As shown in Figure 5, the LUMOs and HOMOs for **2a**−**c** are σ-type orbitals over Pt−Rh−Rh−Pt (**2a**) or Pt−Pt−Rh−Rh−Pt−Pt (**2b** and **2c**). The noteworthy feature is the shapes of HOMO at [Rh−Rh], which is not occupied by sole d_{z^2} orbitals but is occupied by dzx (or dyz), indicating that HOMOs are mixed with π-type orbitals. In other words, in the formation of unbridged Pt−Rh bonds with HOMO−LUMO interactions between Pt_2 σ* and Rh_2 σ* orbitals, the HOMO at Rh_2 π* is also involved with the formation of unbridged bonds.

Figure 6 shows the result of the DFT calculation of **2c**. As mentioned above, both HOMO and LUMO are σ-type orbitals over six metals, where HOMO are antibonding orbitals between Rh_2 σ and two Pt_2 σ* and LUMO are antibonding orbitals between Rh_2 σ* and two Pt_2 σ*. Other σ-type orbitals are found in HOMO − 4 (Figure S8), and more energetically stable ones are expected to attribute to the six aligned metals. The nodes of σ-type orbitals for LUMO, HOMO, and HOMO − 4 are five, four, and three, respectively. In addition, HOMO − 1 and HOMO − 2 are degenerate Rh_2 π* and HOMO − 3 is Rh_2 δ*. Although the order of energetic levels for each molecular orbital is similar, in **na** and **nd** with longer metal−metal distances, σ-

https://doi.org/10.1021/acsomega.1c02634
ACS Omega 2021, 6, 18487−18503

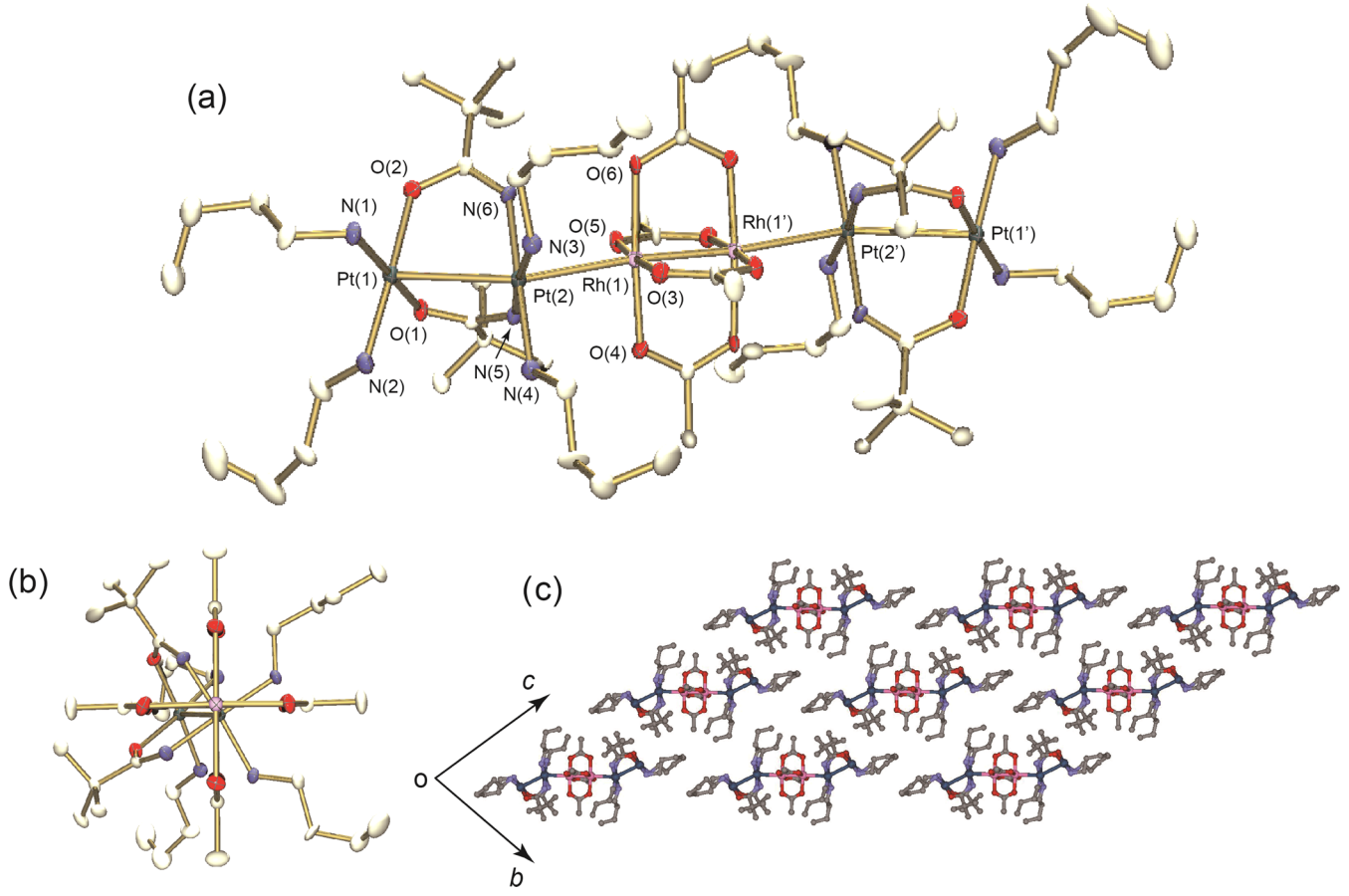

Figure 4. (a) Crystal structure of $[\{Rh_2(O_2CCH_3)_4\}\{Pt_2(piam)_2(NH_2C_4H_9)_4\}_2](ClO_4)_4$ (**5**). (b) Stacking fashion between rhodium dinuclear complex and platinum dinuclear complex in **5**. (c) Packing view of **5**. The hydrogen atoms and anions are omitted for clarity.

Table 1. Comparison of Selected Bond Distances (Å) and Angles (deg) between 1, 2, $[\{Rh_2(O_2CCH_3)_4\}\{Pt_2(piam)_2(NH_2C_2H_5)_4\}_2](PF_6)_4$ (3), $[\{Rh_2(O_2CCH_3)_4\}\{Pt_2(piam)_2(NH_2C_3H_7)_4\}_2](PF_6)_3(ClO_4)$ (4), and $[\{Rh_2(O_2CCH_3)_4\}\{Pt_2(piam)_2(NH_2C_4H_9)_4\}_2](ClO_4)_4$ (5)

compounds	Rh−Rh (Å)	Rh−Pt (Å)	Pt−Pt (Å)	θ_1 (deg)	θ_2 (deg)
1	2.3832(17)	2.7460(10)	2.9376(7)	177.75(6)	156.45(3)
2	2.3779(17)	2.7493(12)	2.9929(10)	177.04(5)	156.93(2)
3	2.3935(8)	2.8321(5)	3.0008(4)	176.68(3)	159.303(11)
4	2.3903(9)	2.7536(6)	2.9356(4)	177.04(3)	159.361(14)
5	2.3920(18)	2.8030(11)	3.0167(10)	174.96(6)	151.84(2)
compounds	ϕ_1 (deg)[a]	ϕ_2 (deg)[a]	ϕ_3 (deg)[a]	τ_1 (deg)	τ_2 (deg)	τ_3 (deg)
1	0	43	8.7	0	1.5	35
2	0	38	16	0	2.4	40
3	0	20	7.5	0	2.6	37
4	0	37	21	0	1.4	36
5	0	32	0.2	0	4.4	36

[a]Average of four angles.

type HOMOs are stabilized to be degenerate with three lower orbitals (Figures S30−S33). These results indicate that depending on metal−metal distances and twist angles between [Rh−Rh] and [Pt−Pt], HOMOs in hexanuclear Pt−Pt−Rh−Rh−Pt−Pt complexes are flexible.

Figure 7 shows the energy levels of molecular orbitals for **2c**, **3c**, **4c**, and **5c**. Although the bridging ligand at the platinum parts did not affect the energy levels (Figures S30−S33), as alkyl groups in co-ligands at platinum atoms become longer, the overall orbital energy increases, but is only due to the change in composition. The HOMO−LUMO gaps in four compounds are similar: 3.12 (**2c**) eV, 3.02 (**3c**) eV, 3.02 (**4c**) eV, and 3.00 (**5c**) eV.

Figure 8 shows diffuse reflection spectra for **1**−**5**. In **1** and **2**, three characteristic absorptions E_1, E_2, and E_3 were observed,[51,58] which are also found in **3**−**5**. Taking into account the fact that the metal oxidation number of the hexanuclear unit in **1**−**5** is $[Pt(+2)_2]-[Rh(+2)_2]-[Pt(+2)_2]$, six molecular orbitals are made from all possible combinations of the metal σ orbitals, $\sigma(Pt_2)-\sigma(Rh_2)-\sigma(Pt_2)$, $\sigma(Pt_2)-\sigma^*(Rh_2)-\sigma(Pt_2)$, $\sigma(Pt_2)-\sigma(Rh_2)-\sigma(Pt_2)$, $\sigma^*(Pt_2)-\sigma^*(Rh_2)-\sigma^*(Pt_2)$, $\sigma^*(Pt_2)-\sigma(Rh_2)-\sigma^*(Pt_2)$, and $\sigma^*(Pt_2)-\sigma^*(Rh_2)-\sigma^*(Pt_2)$,

https://doi.org/10.1021/acsomega.1c02634
ACS Omega 2021, 6, 18487−18503

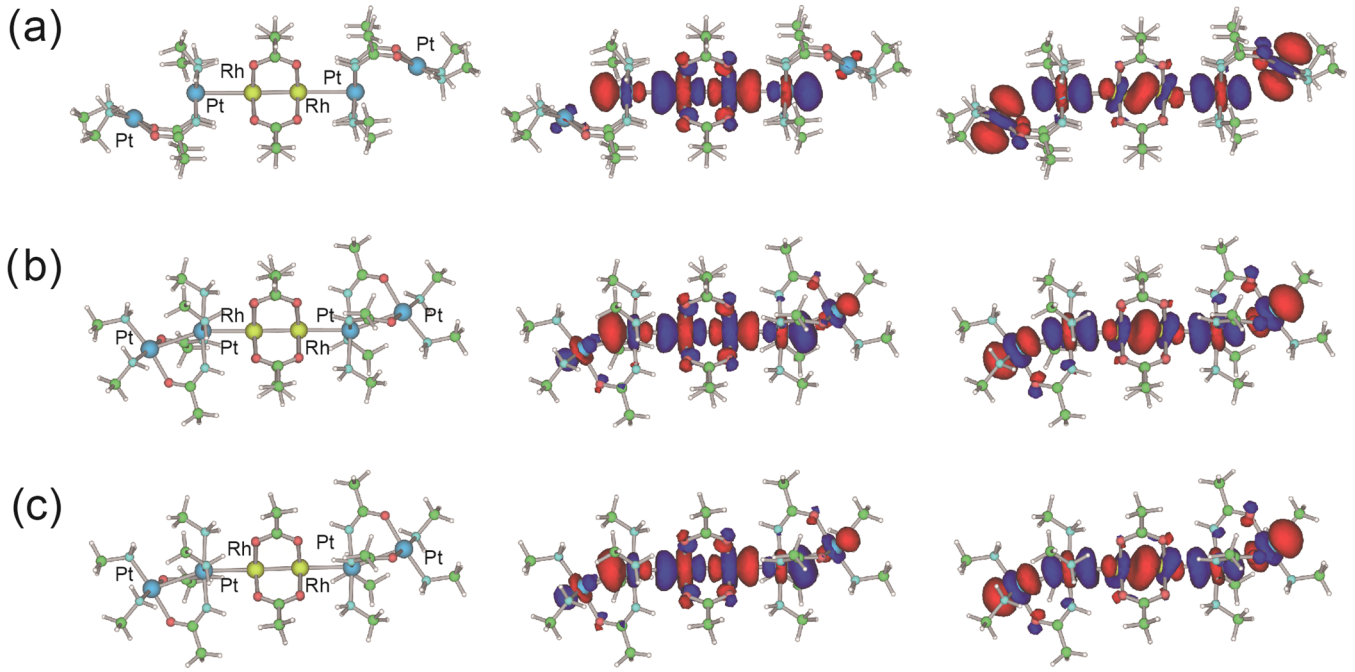

Figure 5. Optimized structures (left), LUMO (middle), and HOMO (right) obtained by DFT calculations based on the model of $[\{Rh_2(O_2CCH_3)_4\}\{Pt_2(NHCOCH_3)_2(NH_2CH_3)_4\}_2]^{4+}$, (a) **2a**, (b) **2b** under the rigid condition of Pt and Rh coordinates, and (c) **2c** under the rigid condition of Pt, Rh, O, and N coordinates.

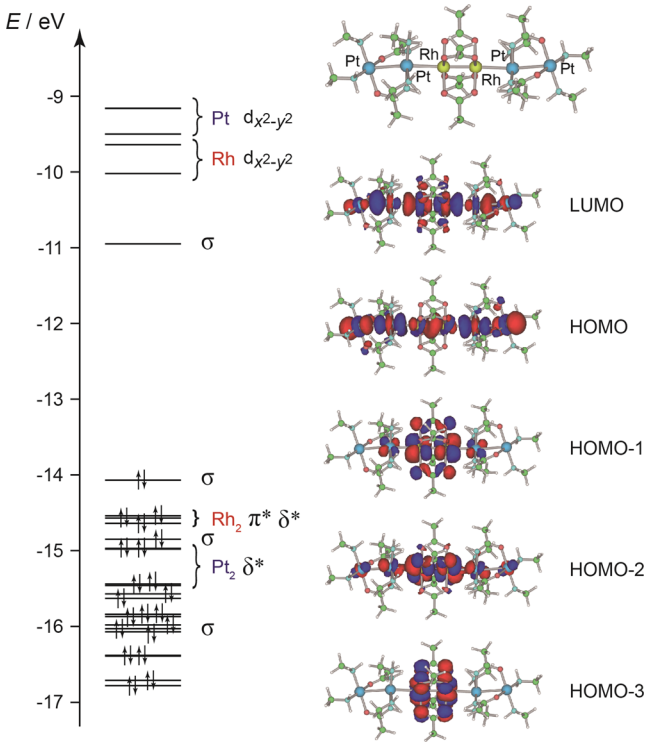

Figure 6. Result of DFT calculation based on the model of $[\{Rh_2(O_2CCH_3)_4\}\{Pt_2(NHCOCH_3)_2(NH_2CH_3)_4\}_2]^{4+}$ (**2c**) under the rigid condition of Pt, Rh, O, and N coordinates.

where energy increases with the number of nodes along the chain direction.[70] As shown in the result of the DFT calculation (Figures 6 and 7), the LUMO comprises $\sigma^*(Pt_2)-\sigma^*(Rh_2)-\sigma^*(Pt_2)$ having all antibonding combinations of $\sigma^*(Pt_2)$ and $\sigma^*(Rh_2)$. Previous analyses[50,55] suggested that E_1 is attributed to the transition from filled σ-type to vacant σ-type orbitals, whereas both E_2 and E_3 are attributed to transition from degenerate Rh_2 π^* to vacant σ-type orbitals. In addition, Figure 9 shows the results of time-dependent density functional theory (TD-DFT) calculations for **5a−c** as bars. The calculated results of TD-DFT for E_1 well coincide the observed results, indicating that the strong absorption in the 2.88−3.05 eV regions is induced by the transition between σ-type orbitals. In **1**, a broad shoulder was observed around 2.60 eV (Figure 8a). Since this broad shoulder is not present in **2−5**, it is attributed to the formation of a band structure. In other words, the appearance of the shoulder band in **1** proved the significant interaction between end Pt and Pt atoms of hexanuclear Pt−Pt−Rh−Rh−Pt−Pt units. Among **2−5**, the values of E_1 are similar or slightly decreased with longer chain of alkyl groups at co-ligands.

Although E_1 is exactly assigned by the TD-DFT calculations, the estimation of both E_2 and E_3 is difficult. Results of TD-DFT calculations for **5a−c** showed weak adsorption around <2.0 eV, which are caused by the transition from HOMO − 1 and HOMO − 2 of degenerate Rh_2 π^* to LUMO admixed with transitions from HOMO to LUMO. The absorption of E_2 in lower energetic regions attributed to wider transition from HOMO − 1 to LUMO than HOMO to LUMO is conflicting; a probable reason for this is that calculated energy levels are based on static structures, and they do not consider local differences of structures caused by vibrations. In reality, in $[\{Rh_2(O_2CCH_3)_4\}\{Pt_2Cu(piam)_4(NH_3)_4\}]_n(PF_6)_{2n}$[55] and $[\{Rh_2(O_2CCH_3)_4\}\{Pt_2Co(piam)_4(NH_3)_4\}]_n(PF_6)_{2n}$[56] with staggered and eclipsed stacking between Pt and Rh coordination planes, respectively, the peak strengths of both E_2 and E_3 in the latter are weaker than those in the former,[56] depending on twist angles between the two complexes. As shown in Figure 8d,e, absorption peaks of E_3 in **4** and **5** were not observed. Since the energetic differences between E_2 and E_3 observed in **1−3** are small and similar, the observation of E_3 is related to whether Rh_2 π^* is degenerate or not. This trend evidently revealed that both E_2 and E_3 are involved with degenerate Rh_2 π^* orbitals.

https://doi.org/10.1021/acsomega.1c02634
ACS Omega 2021, 6, 18487−18503

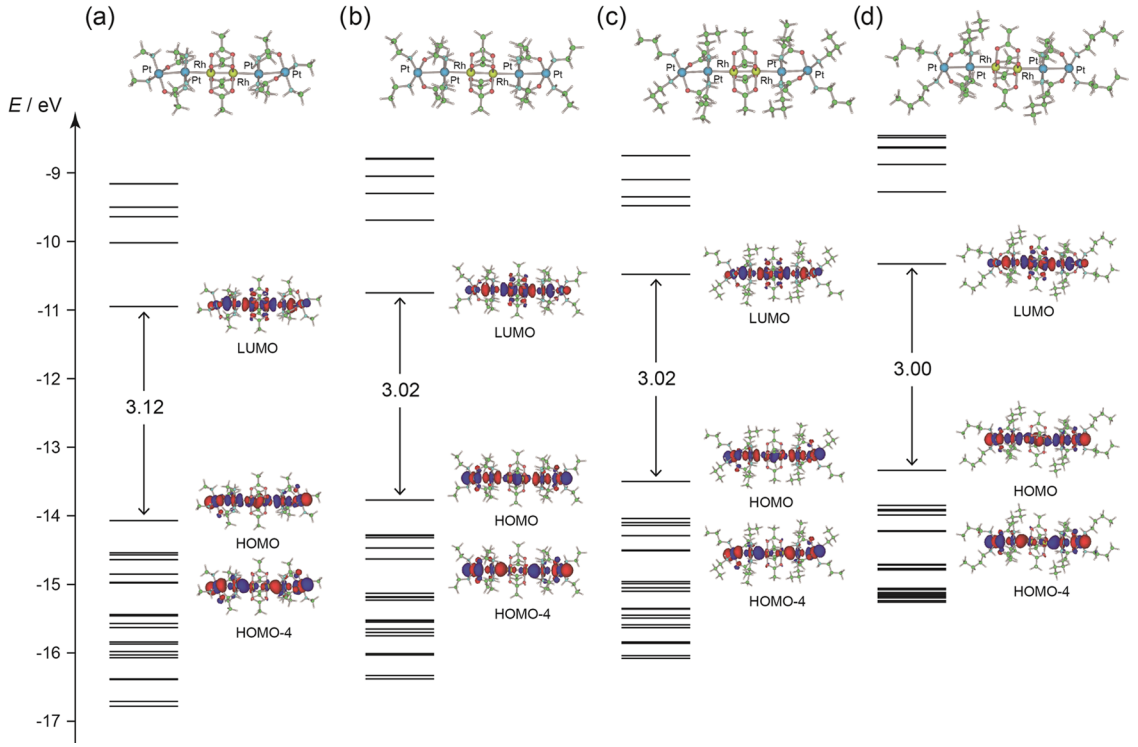

Figure 7. Results of DFT calculation based on the model of (a) $[\{Rh_2(O_2CCH_3)_4\}\{Pt_2(NHCOCH_3)_2(NH_2CH_3)_4\}_2]^{4+}$ (**2c**), (b) $[\{Rh_2(O_2CCH_3)_4\}\{Pt_2(NHCOCH_3)_2(NH_2C_2H_5)_4\}_2]^{4+}$ (**3c**), (c) $[\{Rh_2(O_2CCH_3)_4\}\{Pt_2(NHCOCH_3)_2(NH_2C_3H_7)_4\}_2]^{4+}$ (**4c**), and (d) $[\{Rh_2(O_2CCH_3)_4\}\{Pt_2(NHCOCH_3)_2(NH_2C_4H_9)_4\}_2]^{4+}$ (**5c**).

Stabilities of Hexanuclear Structures in Nonpolar Solvents. In general, the molecule with longer alkyl chains has more hydrophobicity. The previously reported trinuclear Pt−Cu−Pt complexes comprising propyl or butylamine coordinated to end Pt atoms are soluble in nonpolar solvents, such as CH_2Cl_2, although they are cationic complexes.[61] In these trinuclear complexes aligned as Pt−Cu−Pt, each metal is bridged by piam ligands. In contrast, hexanuclear **2**−**5** have two unbridged Pt−Rh bonds. When compounds **2**−**5** are immersed in polar solvents, such as MeOH, most of the hexanuclear molecules are dissociated to afford dinuclear complexes, due to the coordination of solvent molecules. Figure 10 shows ESI-MS spectra of the MeOH solution containing **4** or **5**. In **4**, weak signals at m/z = 1897, 1943, 2339, and 2385 corresponding to $\{[Pt_2(piam)_2(NH_2C_3H_7)_4]_2(PF_6)(ClO_4)-H\}^+$, $\{[Pt_2(piam)_2(NH_2C_3H_7)_4]_2(PF_6)_2-H\}^+$, $\{[\{Rh_2(O_2CCH_3)_4\}\{Pt_2(piam)_2(NH_2C_3H_7)_4\}_2](PF_6)(ClO_4)-H\}^+$, and $\{[\{Rh_2(O_2CCH_3)_4\}\{Pt_2(piam)_2(NH_2C_3H_7)_4\}_2](PF_6)_2-H\}^+$ were observed. Furthermore, in **5**, weak signals at m/z = 2110, 2155, 2201, 2260, 2305, and 2351 corresponding to $\{[Pt_2(piam)_2(NH_2C_4H_9)_4]_2(PF_6)(ClO_4)_2\}^+$, $\{[Pt_2(piam)_2(NH_2C_4H_9)_4]_2(PF_6)_2(ClO_4)\}^+$, $\{[Pt_2(piam)_2(NH_2C_4H_9)_4]_2(PF_6)_3\}^+$, $\{[\{Rh_2(O_2CCH_3)_4\}\{Pt_2(piam)_2(NH_2C_4H_9)_3\}_2](ClO_4)_2-H\}^+$, $\{[\{Rh_2(O_2CCH_3)_4\}\{Pt_2(piam)_2(NH_2C_4H_9)_3\}_2](PF_6)(ClO_4)-H\}^+$, and $\{[\{Rh_2(O_2CCH_3)_4\}\{Pt_2(piam)_2(NH_2C_4H_9)_3\}_2](PF_6)_2-H\}^+$ were observed. Both **4** and **5** contained PF_6^- and ClO_4^- as counter anions, which are mixed during synthetic and crystallized processes; both anions have similar molecular sizes and spherical shapes.[74,75] Although hexanuclear units of **4** and **5** are observed in MeOH, indicating the partial maintenance of their hexanuclear backbones, the unbridged Pt−Rh bonds are dissociated by the MeOH molecules.

Furthermore, both **4** and **5** have enough solubilities in CH_2Cl_2. Figure 11 shows the ultraviolet−visible (UV−vis) spectra of the CH_2Cl_2 solution containing **4** or **5** with their photograph, in comparison to the results of diffuse reflection spectra (Figure 8d,e). In both **4** and **5**, three absorption peaks were observed at 356, 427 (452), and 692 nm for **4** and at 363, 429, and 690 nm for **5**. The energetically highest peaks at 356 (**4**) and 363 (**5**) were also found in their solid state as submaxima peaks, although the measured range was out of resolution for our instrument system. Both 427 (**4**) and 429 (**5**) well coincide with 420 (=2.95 eV, **4**) and 430 (=2.88 eV, **5**), which correspond to E_1. Moreover, E_2 was found at 692 (**4**) and 690 (**5**). The spectra of the solution and solid states well coincide, revealing that both **4** and **5** maintain their hexanuclear backbones in CH_2Cl_2.

The UV−vis spectra of MeOH solution containing $[Rh_2(O_2CCH_3)_4]$ and $[Pt_2(piam)_2(NH_2R)_4](PF_6)_2$ (R = C_3H_7 or C_4H_9), which are the starting materials for **4** and **5**, in different ratios show no absorption peaks (Figure S34a,c), indicating that two complexes do not associate in MeOH. However, in CH_2Cl_2, as $[Pt_2(piam)_2(NH_2R)_4](PF_6)_2$ are added, absorption peaks around 300−450 nm become intense, indicating that the two complexes do associate. In both cases, however, the absorbances of the E_1 absorption at 420 (**4**) and 430 nm (**5**), which are characteristic for the formation of hexanuclear backbones, are low. Considering that the growing peaks are observed at lower wavelengths, mixing two complexes in CH_2Cl_2 dominantly affords tetranuclear complexes, $[Rh_2]-[Pt_2]$.

Figure 12 shows the ^1H NMR spectrum of the hexanuclear complex **5** dissolved in CD_2Cl_2. In addition to the CH_3 group of

https://doi.org/10.1021/acsomega.1c02634
ACS Omega 2021, 6, 18487−18503

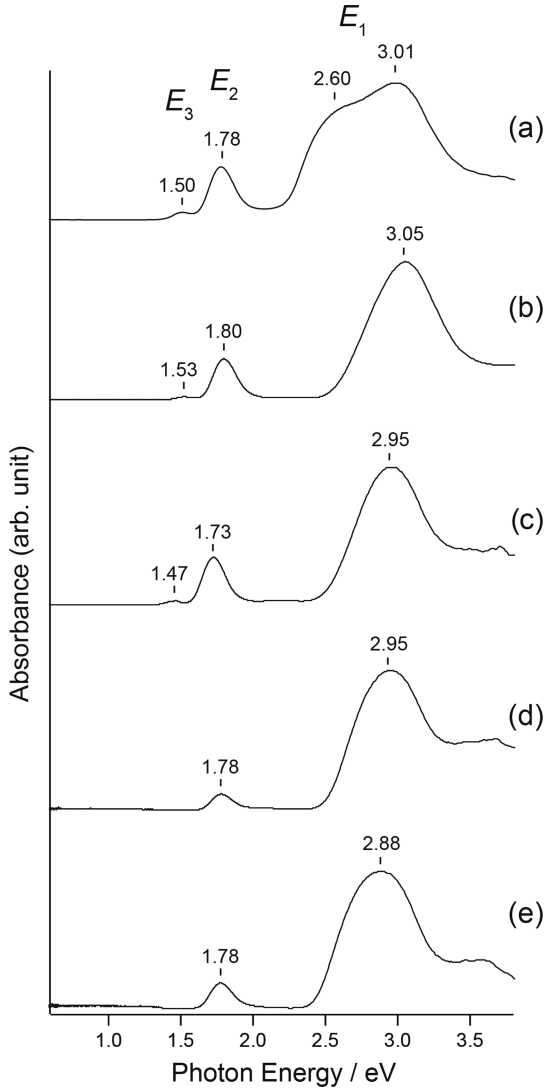

Figure 8. Diffuse reflectance spectra of (a) **1**, (b) **2**, (c) **3**, (d) **4**, and (e) **5** with MgO at room temperature.

$[Rh_2(O_2CCH_3)_4]$ and the ^{t}Bu group of $[Pt_2(piam)_2(NH_2C_4H_9)_4]^{2+}$, the C_4H_9 groups were observed as broad peaks. For all four kinds of proton, sharper (a−d) and broader (a′−d′) peaks were observed at the lower and higher fields, respectively. The broader peaks (*a*′−*d*′) are attributed to the inner butylamine in the hexanuclear complex, due to the inhibition of free rotation in the molecule, whereas the sharper peaks (*a*−*d*) are attributed to the outer butylamine, where the integral values well coincided with the chemical formula.

As shown in Figure 13, ^{1}H NMR and UV−vis spectra of **5** with 3 equiv of $[Pt_2(piam)_2(NH_2C_4H_9)_4](PF_6)_2$ showed no significant change from those of **5**. Therefore, the dissociation of **5** is suppressed in CH_2Cl_2, maintaining the hexanuclear backbone. Despite the cationic hexanuclear complexes, the reason of solubility in CH_2Cl_2 is the hydrophobic interaction of propyl or butyl moieties at amine ligands coordinated Pt atoms. Considering the crystal structures (Figure 4), the eight alkyl chains avoid the dissociation of the unbridged Pt−Rh bonds by surrounding their molecules (Scheme 4). Thus, soluble hexanuclear Pt−Pt−Rh−Rh−Pt−Pt units were successfully appeared as if HMSCs from infinite heterometallic 1D chains **1** aligned as $-\{Pt-Pt-Rh-Rh-Pt-Pt\}_n-$. Similar measurements were also carried out for hexanuclear complex **4** (Figures S35 and S36). When 3 equiv $[Pt_2(piam)_2(NH_2C_3H_7)_4](PF_6)_2$ were added to **4**, although a similar trend was observed, indistinguishable peaks appeared in ^{1}H NMR spectra and absorption peaks are slightly shifted to lower wavelengths in the UV−vis spectra. These results suggest that the hexanuclear complex **4** with propylamine is in an equilibrium reaction with some dissociation even in CH_2Cl_2.

The direct benefit of the solubility of compounds without changes to their molecular structures is the extension of the experimental approach to solution states. For example, Figure 14 shows cyclic voltammograms of **4** and **5** recorded with CH_2Cl_2 solution containing 0.1 M Bu_4NPF_6 as a supporting electrolyte, in comparison of the cyclic voltammograms of $[Rh_2(O_2CCH_3)_4(CH_3CN)_2]$. In $[Rh_2(O_2CCH_3)_4(CH_3CN)_2]$, a reversible wave at $E_{1/2}$ = 0.62 V (vs Fc/Fc^+) was observed, which are attributed to one-electron oxidation and reduction at the Rh_2 π^* orbital.[76−78] In contrast, both **4** and **5** afford the quasi-reversible oxidation and reduction waves at **4**: E_{ox} = 0.86 V and E_{red} = 0.69 V and **5**: E_{ox} = 0.87 V and E_{red} = 0.53 V. As shown in Figure S37, there are no significant oxidation waves in the cyclic voltammograms of the mononuclear or dinuclear Pt complexes, *cis*-$[Pt(piam)_2(NH_2C_3H_7)_2]\cdot H_2O$, $[Pt_2(piam)_2(NH_2C_3H_7)_4](PF_6)_2$, *cis*-$[Pt(piam)_2(NH_2C_4H_9)_2]$, and $[Pt_2(piam)_2(NH_2C_4H_9)_4](PF_6)_2$, which are the modules for **4** and **5**. The difficulty is probably due to that the oxidation of Pt(+2) atom is involved with the axial coordination.[79] Considering the results of DFT calculation, the oxidation and reduction of **4** and **5** occurred at HOMOs, which consist of σ^* over the hexanuclear metals admixed with Rh_2 π^*. Using the obtained E_{ox} values, the absolute values of E_{HOMO} were successfully estimated as −5.66 (**4**) eV and −5.67 (**5**) eV, according to the equation of E_{HOMO} (eV) = −(4.8 + E_{ox} (V vs Fc/Fc^+)).[80−82] Furthermore, for **5**, electron paramagnetic resonance (EPR) measurement was conducted after the electrolytic oxidation. The CH_2Cl_2 solution containing 1 mM **5** with 0.1 M Bu_4NPF_6 as supporting electrolyte was electrolytically oxidized and immediately frozen under 77 K. The EPR spectrum for the CH_2Cl_2 glass shows a broad isotropic signal with g = 2.52 (Figure S38). Considering that the value of g is higher than the spin-only value, the unpaired electron was affected by the significant spin−orbit coupling from the metals, resulting in that HOMO of **5** is on the metal, which coincided with the calculations. We also tried to chemically oxidize **5** with I_2 or H_2O_2 but did not succeeded in isolating. Hence, we performed an one-electron oxidized DFT calculation based on the model **2c** with a different charge, $[\{Rh_2(O_2CCH_3)_4\}\{Pt_2(NHCOCH_3)_2(NH_2CH_3)_4\}_2]^{5+}$ (**2c**$^+$), under the rigid condition of Pt, Rh, O, and N coordinates (Figure S39). As shown in Figure 15, the molecular orbital corresponding to the SOMO was not different from the HOMO of **2c**, but was a mixture of σ^* delocalized in the hexanuclear metal and Rh_2 π^* orbitals.

CONCLUSIONS

This study demonstrated the syntheses and characterization of hexanuclear complexes as novel HMSCs containing two unbridged metal−metal bonds constructed by the HOMO−LUMO interaction at d_{z^2} orbitals. By introducing alkyl moieties at co-ligand-coordinated Pt atoms, further extension was obstructed, and the obtained hexanuclear complexes appeared as if they were excised from the prototype heterometallic 1D chain **1**. Comparing the infinite chain **1** with hexanuclear **2**−**5**,

https://doi.org/10.1021/acsomega.1c02634
ACS Omega 2021, 6, 18487−18503

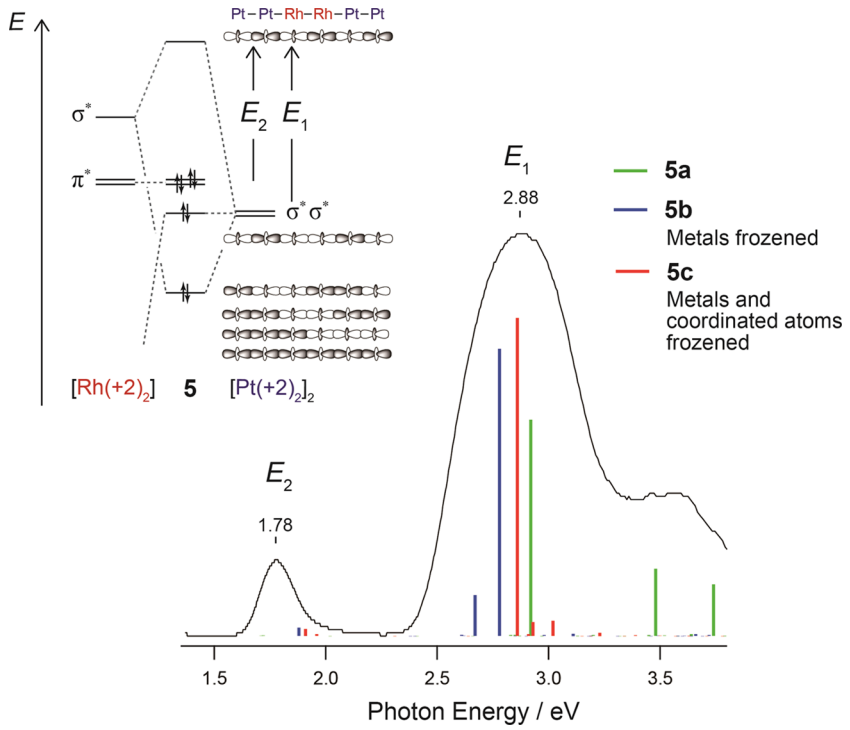

Figure 9. Diffuse reflectance spectra of **5** with schematic electronic structure. Green, blue, and red bars show the results of TD-DFT calculation for **5a**, **5b**, and **5c**, respectively.

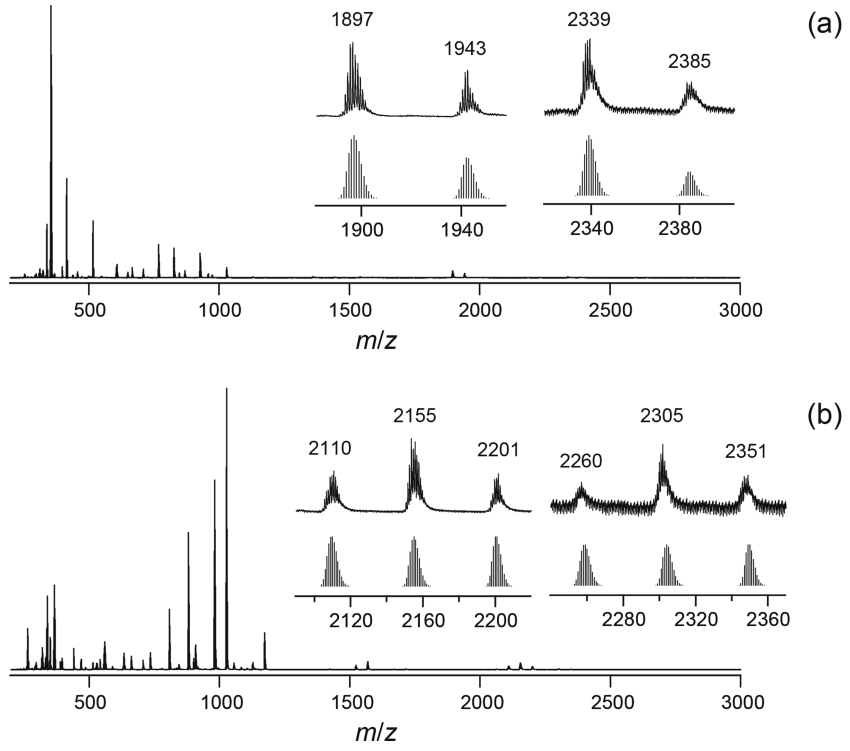

Figure 10. ESI-MS (positive) spectra for (a) **4** and (b) **5** measured by dilution in MeOH. Selected peaks are simulated with isotope patterns as bars.

unclear problems for **1** were revealed, such as shoulder absorption around E_1 attributed to band structure or exact molecular orbitals. Interestingly, when the alkyl moieties were propyl or butyl, hydrophobic interaction provided enough solubility in nonpolar solvents. In addition to the infinite chains in solid state, the HOMO−LUMO interactions at d_{z^2} orbitals are effective for HMSCs, comprising unique compounds with various numbers of metal and metal species.

EXPERIMENTAL SECTION

Materials. Rhodium(III) chloride trihydrate and potassium tetrachloroplatinate(II) were obtained from Tanaka Kikinzoku Co. 40% NH_2CH_3 aqua solution, 70% $NH_2C_2H_5$ aqua solution,

https://doi.org/10.1021/acsomega.1c02634
ACS Omega 2021, 6, 18487−18503

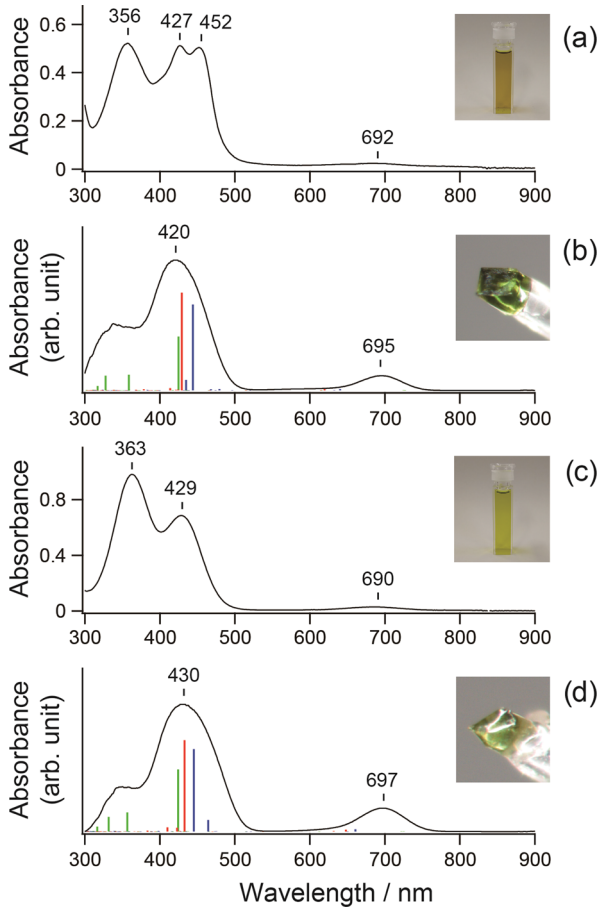

Figure 11. UV−vis spectra of 0.05 mM CH_2Cl_2 solution containing (a) **4** and (c) **5**. Diffuse reflectance spectra of (b) **4** and (d) **5** with MgO at room temperature. Green, blue, and red bars show the results of TD-DFT calculation for **na**, **nb**, and **nc**, respectively. Photograph courtesy of "Kazuhiro Uemura". Copyright 2021.

$NH_2C_4H_9$, $NaClO_4$, and KI were obtained from Nacalai Tesque Co. $NaPF_6$, pivalonitrile, and $NH_2C_3H_7$ were obtained from Tokyo Chemical Industry Co. $AgNO_3$ and $AgPF_6$ were obtained from Wako Co. *cis*-$[PtI_2(NH_2CH_3)_2]$, *cis*-$[PtI_2(NH_2C_2H_5)_2]$, *cis*-$[PtI_2(NH_2C_3H_7)_2]$, and *cis*-$[PtI_2(NH_2C_4H_9)_2]$ were synthe-

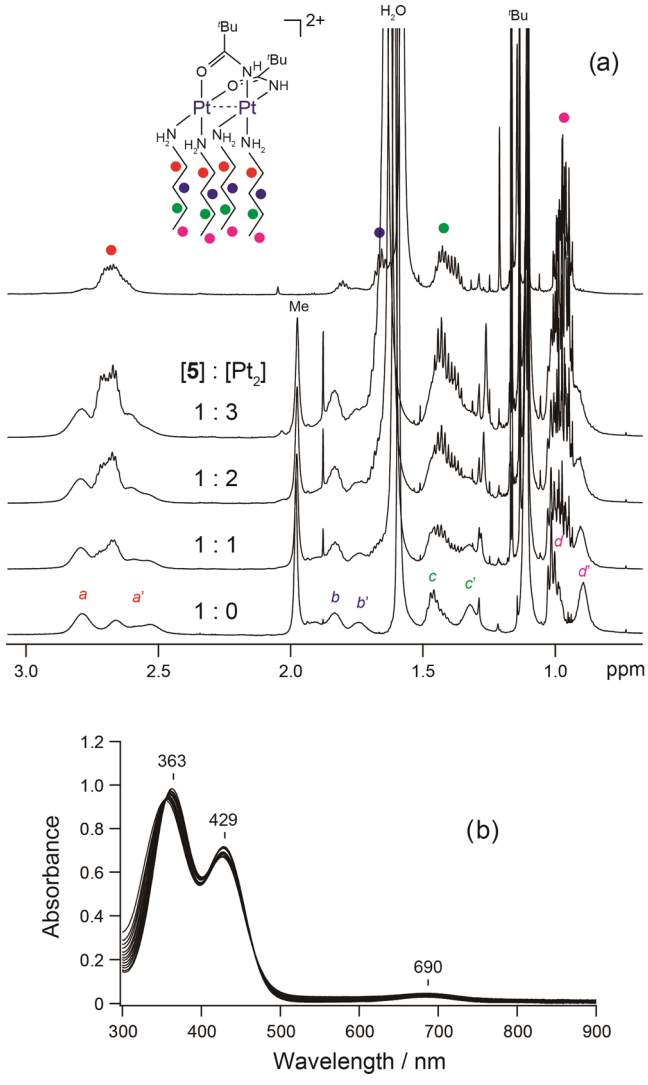

Figure 13. (a) ^{1}H NMR spectra (600 MHz in CD_2Cl_2, 0.5 mM) of **5** with 0, 1, 2, and 3 equiv $[Pt_2(piam)_2(NH_2C_4H_9)_4](PF_6)_2$. (b) UV−vis spectra of 0.05 mM CH_2Cl_2 solution containing **5** with 0, 0.25, 0.5, ..., and 3.0 equiv $[Pt_2(piam)_2(NH_2C_4H_9)_4](PF_6)_2$.

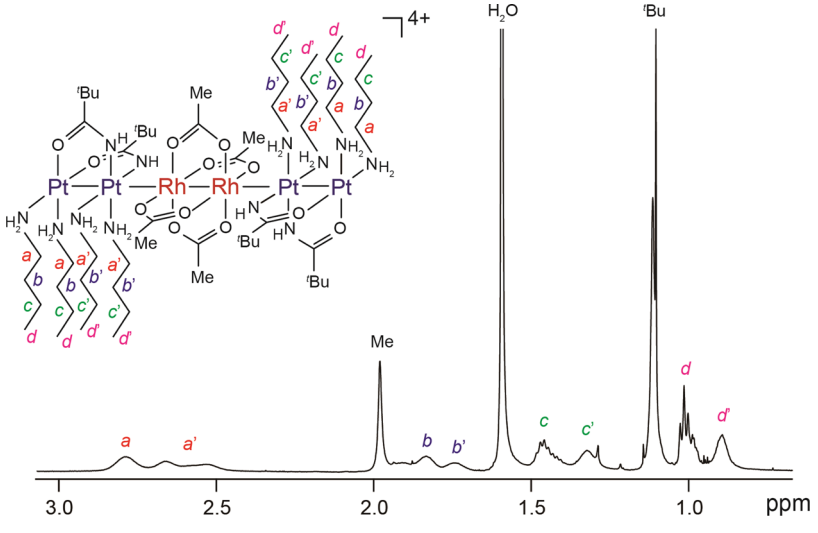

Figure 12. ^{1}H NMR spectrum (600 MHz in CD_2Cl_2, 0.5 mM) of **5**.

https://doi.org/10.1021/acsomega.1c02634
ACS Omega 2021, 6, 18487−18503

Scheme 4. Alkyl Moieties Support the Maintaining of Hexanuclear Backbone in Hydrophobic Solvents

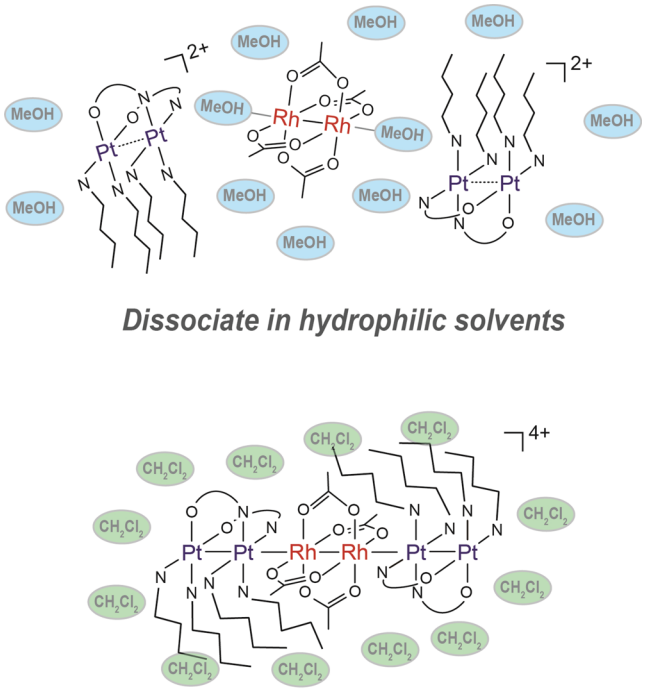

sized by a modified version of Dhara's method.[83,84] *cis*-$[Pt(piam)_2(NH_2CH_3)_2]\cdot H_2O$,[59] *cis*-$[Pt(piam)_2(NH_2C_2H_5)_2]\cdot H_2O$,[60] *cis*-$[Pt(piam)_2(NH_2C_3H_7)_2]\cdot H_2O$,[61] *cis*-$[Pt(piam)_2(NH_2C_4H_9)_2]$,[61] $[Rh_2(O_2CCH_3)_4]$,[85] $[\{Rh_2(O_2CCH_3)_4\}\{Pt_2(piam)_2(NH_3)_4\}_2]_n(PF_6)_{4n}\cdot 6nH_2O$ (**1**),[51] and $[\{Rh_2(O_2CCH_3)_4\}\{Pt_2(piam)_2(NH_2CH_3)_4\}_2](PF_6)_4$ (**2**)[58] were synthesized according to the previous procedures.

Synthesis of $[\{Rh_2(O_2CCH_3)_4\}\{Pt_2(piam)_2(NH_2C_2H_5)_4\}_2](PF_6)_4$ (***3***). An aqueous solution (5 mL) of $[PtI_2(NH_2C_2H_5)_2]$ (0.29 g, 0.54 mmol) was stirred with $AgPF_6$ (0.27 g, 1.1 mmol) overnight in the dark, and AgI was then removed by filtration. The colorless filtrate was evaporated and stirred with *cis*-$[Pt(piam)_2(NH_2C_2H_5)_2]\cdot H_2O$ (0.26 g, 0.52 mmol) in MeOH (5 mL) for 2.5 h. The resulting light yellow solution was evaporated to obtain crude $[Pt_2(piam)_2(NH_2C_2H_5)_4](PF_6)_2$ (0.38 g). A EtOH solution (0.75 mL) of crude powder (9.6 mg) was layered on a EtOH solution (0.75 mL) of $[Rh_2(O_2CCH_3)_4]$ (2.2 mg, 5.0 μmol). After several days, yellow-green crystals with metallic luster were obtained (5.2 mg). Yield 41%. Elemental analysis calcd for $C_{44}H_{108}F_{24}N_{12}O_{12}P_4Pt_4Rh_2$: C, 20.62; H, 4.25; N, 6.56%, found: C, 21.10; H, 4.38; N, 6.74%.

Synthesis of $[\{Rh_2(O_2CCH_3)_4\}\{Pt_2(piam)_2(NH_2C_3H_7)_4\}_2](PF_6)_3(ClO_4)$ (***4***). An aqueous solution (5 mL) of $[PtI_2(NH_2C_3H_7)_2]$ (0.32 g, 0.56 mmol) was stirred with $AgPF_6$ (0.28 g, 1.1 mmol) overnight in the dark, and AgI was then removed by filtration. The colorless filtrate was evaporated and stirred with *cis*-$[Pt(piam)_2(NH_2C_3H_7)_2]\cdot H_2O$ (0.29 g, 0.55 mmol) in MeOH (7 mL) for 2.5 h. The resulting light blue solution was evaporated to obtain crude $[Pt_2(piam)_2(NH_2C_3H_7)_4](PF_6)_2$ (0.51 g). An EtOH solution (1.0 mL) of crude powder (7 mg), $[Rh_2(O_2CCH_3)_4]$ (1 mg, 2.3 μmol), and $NaClO_4$ (0.4 mg, 3.3 μmol) layered on H_2O (3.0 mL) was slowly evaporated. After several days, green crystals with metallic luster were obtained (2 mg). Yield 33%. Elemental analysis calcd for $C_{52}H_{124}ClF_{18}N_{12}O_{16}P_3Pt_4Rh_2$: C, 23.75; H, 4.75; N, 6.39%, found: C, 23.86; H, 4.79; N, 6.43%.

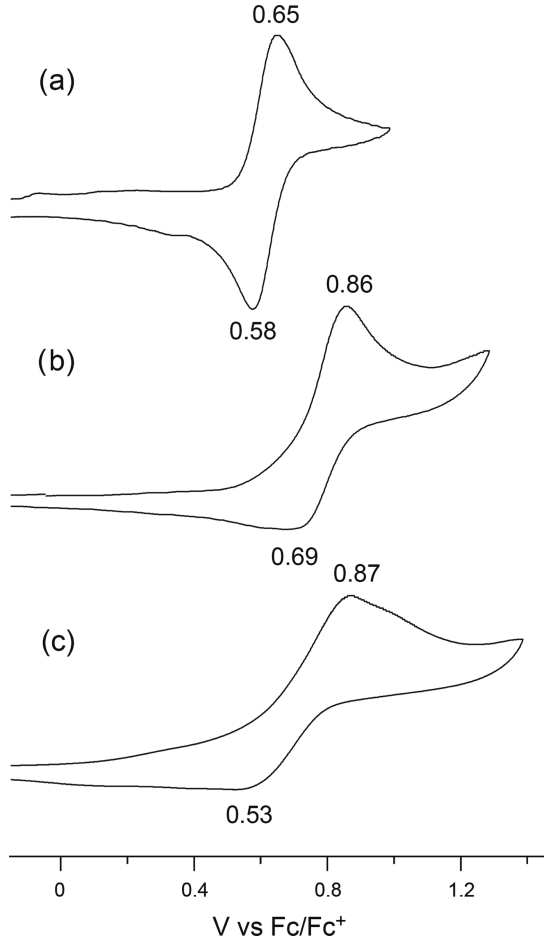

Figure 14. Cyclic voltammograms of (a) $[Rh_2(O_2CCH_3)_4(CH_3CN)_2]$ in CH_3CN, (b) **4**, and (c) **5** in CH_2Cl_2 in the presence of 0.1 M Bu_4NPF_6 as the supporting electrolyte (scan rate: 100 mV s^{-1}). The values are given with regard to Fc/Fc^+, which has been used as internal standard for calibration of the Ag/AgCl reference electrode.

Synthesis of $[\{Rh_2(O_2CCH_3)_4\}\{Pt_2(piam)_2(NH_2C_4H_9)_4\}_2](ClO_4)_4$ (***5***). An aqueous solution (5 mL) of $[PtI_2(NH_2C_4H_9)_2]$ (0.29 g, 0.49 mmol) was stirred with $AgPF_6$ (0.24 g, 0.95 mmol) for overnight in the dark, and AgI was then removed by filtration. The colorless filtrate was evaporated and stirred with *cis*-$[Pt(piam)_2(NH_2C_4H_9)_2]$ (0.26 g, 0.48 mmol) in MeOH (7 mL) for a day. The resulting brown solution was evaporated to obtain crude $[Pt_2(piam)_2(NH_2C_4H_9)_4](PF_6)_2$ (0.38 g). An EtOH solution (1.0 mL) of crude powder (7 mg), $[Rh_2(O_2CCH_3)_4]$ (1 mg, 2.3 μmol), and $NaClO_4$ (0.4 mg, 3.3 μmol) layered onH_2O (3.0 mL) was slowly evaporated. After several days, green crystals with metallic luster were obtained (3.0 mg). Yield 50%. Elemental analysis calcd for $C_{60}H_{140}Cl_4N_{12}O_{28}Pt_4Rh_2$: C, 27.66; H, 5.42; N, 6.45%, found: C, 28.03; H, 5.61; N, 6.57%. As mentioned in the text, bulk synthesized product contains several amounts of PF_6^- instead of ClO_4^-.

Physical Measurements. UV−vis spectra were recorded using a Shimadzu UV3100PC at room temperature. The XPS measurements were carried out on a Quantera-SXM spectrometer at room temperature. Binding energies were measured relative to the C 1s peak (284.8 eV) of an internal hydrocarbon.

https://doi.org/10.1021/acsomega.1c02634
ACS Omega 2021, 6, 18487−18503

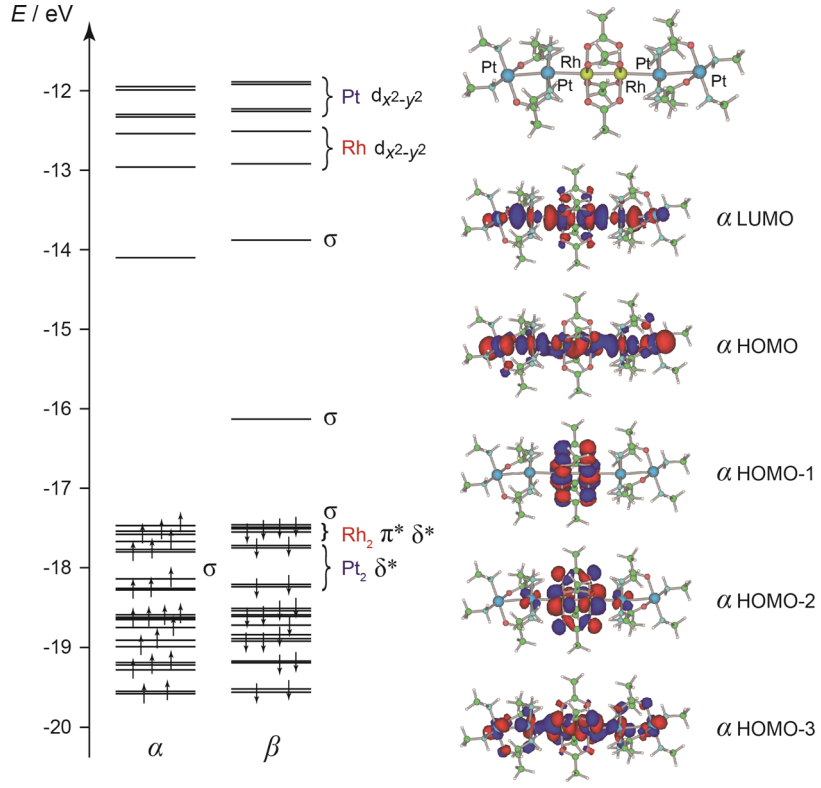

Figure 15. Result of DFT calculation based on the model of $[\{Rh_2(O_2CCH_3)_4\}\{Pt_2(NHCOCH_3)_2(NH_2CH_3)_4\}_2]^{5+}$ ($\mathbf{2c}^+$) under the rigid condition of Pt, Rh, O, and N coordinates.

Table 2. Crystallographic Data and Structure Refinements for $[\{Rh_2(O_2CCH_3)_4\}\{Pt_2(piam)_2(NH_2C_2H_5)_4\}_2](PF_6)_4$ (3), $[\{Rh_2(O_2CCH_3)_4\}\{Pt_2(piam)_2(NH_2C_3H_7)_4\}_2](PF_6)_3(ClO_4)$ (4), and $[\{Rh_2(O_2CCH_3)_4\}\{Pt_2(piam)_2(NH_2C_4H_9)_4\}_2](ClO_4)_4$ (5)

	3	4	5
empirical formula	$C_{44}H_{108}F_{24}N_{12}O_{12}P_4Pt_4Rh_2$	$C_{52}H_{124}F_{18}N_{12}O_{14}P_3Pt_4Rh_2$	$C_{60}H_{140}Cl_4N_{12}O_{28}Pt_4Rh_2$
formula weight	2563.48	2562.71	2605.81
crystal system	monoclinic	triclinic	triclinic
space group	$C2/c$	$P\bar{1}$	$P\bar{1}$
a (Å)	35.658(4)	12.6800(16)	10.799(3)
b (Å)	12.1247(13)	12.8383(15)	14.482(4)
c (Å)	20.754(3)	15.356(2)	15.787(5)
α (deg)	90	80.918(5)	77.164(9)
β (deg)	119.4765(14)	89.778(6)	89.966(11)
γ (deg)	90	64.518(3)	77.378(8)
V (Å^3)	7811.6(16)	2222.5(5)	2346.1(12)
Z	4	1	1
temperature (K)	123	123	123
D_c (Mg m^{-3})	2.180	1.915	1.844
absorption coefficient (mm^{-1})	7.745	6.781	6.471
F(000)	4920	1241	1278
crystal size (mm^3)	0.30 × 0.20 × 0.10	0.30 × 0.25 × 0.10	0.20 ×0.10 × 0.10
measured reflections	30 945	17 778	19 015
independent reflections	8941 [R_{int} = 0.0314]	10 024 [R_{int} = 0.0287]	10 576 [R_{int} = 0.0527]
data/restraints/parameters	8941/0/474	10024/0/482	10576/0/508
goodness of fit on F^2	1.066	1.105	1.199
R [$I > 2\sigma(I)$]	0.0347	0.0450	0.0620
R (all data)	0.0387	0.0521	0.0935

The diffuse reflectance spectra were recorded on a Hitachi U-4000 spectrophotometer over the range from 200 to 2500 nm at room temperature. The infrared spectra were recorded on a PerkinElmer Spectrum 400 over the range from 400 to 4000 cm^{-1} at room temperature. Cyclic voltammetric measurements were conducted at room temperature using a BAS CV-50W or BAS 617E electrochemical analyzer. Cyclic voltammograms were recorded with CH_3CN or CH_2Cl_2 solutions containing 0.1 M Bu_4NPF_6 as the supporting electrolyte. Conventional three-electrode arrangement consisting of glassy carbon or Pt working

https://doi.org/10.1021/acsomega.1c02634
ACS Omega 2021, 6, 18487−18503

electrode, Ag/Ag^+ reference electrode, and Pt wire counter electrode was used. EPR spectra were measured on a JEOL TE-200 spectrometer. ^1H NMR were conducted on a JEOL ECA-600.

Density Functional Theory (DFT) Calculation. The electronic structures of model compound $[\{Rh_2(O_2CCH_3)_4\}\{Pt_2(NHCOR')_2(NH_2R)_4\}_2]^{4+}$ (R = CH_3, C_2H_5, C_3H_7 or C_4H_9, R′ = CH_3 or ^{t}Bu) were determined using the DFT method with the B3LYP function[86−88] and Gaussian 16 program package.[89] For Pt and Rh, LANL2DZ basis set was used together with the effective core potential of Hay and Wadt.[90] For the other elements, 6-31G* basis sets[91] were selected. The initial models of $[\{Rh_2(O_2CCH_3)_4\}\{Pt_2(NHCOR')_2(NH_2R)_4\}_2]^{4+}$ for optimization were prepared using the geometrical parameters obtained from the crystal structure data. For the models, full geometry optimization was conducted without rigid condition, under the rigid condition of coordinates for the metal, or under the rigid condition of coordinates for the metal and coordination atoms. Based on structure, 40 singlets in excited state were obtained to determine vertical excitation energy using time-dependent (TD) DFT calculation.[92,93]

X-ray Structure Determination. Measurements were carried out on a Rigaku AFC7R Mercury CCD diffractometer equipped with a normal-focus Mo-target X-ray tube (λ = 0.7107 Å) operated at 15 kW power (50 kV, 300 mA) and a CCD two-dimensional detector. A total of 744 frames were collected with a scan width of 0.5° with an exposure time of 5 s/frame. Empirical absorption correction[94] were performed for all data. The structure was solved by direct method[95] with subsequent difference Fourier synthesis and refinement using SHELX-2017[96] controlled by a Yadokari-XG software package.[97] Nonhydrogen atoms were refined anisotropically and all hydrogen atoms were treated as riding atoms. In **4**, the oxygen atom O7 of water molecule was refined isotropically without hydrogen atoms. The crystal data and structure refinement results are summarized in Table 2.

■ ASSOCIATED CONTENT

Supporting Information

The Supporting Information is available free of charge at https://pubs.acs.org/doi/10.1021/acsomega.1c02634.

Crystal structures; IR spectra; XPS; DFT calculation; ^1H NMR; UV−vis spectra; cyclic voltammograms; EPR spectrum (PDF)

Crystallographic data CCDC 2051161 (CIF)

Crystallographic data CCDC 2051162 (CIF)

Crystallographic data CCDC 2051163 (CIF)

■ AUTHOR INFORMATION

Corresponding Author

Kazuhiro Uemura − *Department of Chemistry and Biomolecular Science, Faculty of Engineering, Gifu University, Gifu 501-1193, Japan;* orcid.org/0000-0001-9926-9306; Email: k_uemura@gifu-u.ac.jp

Authors

Erina Yasuda − *Department of Chemistry and Biomolecular Science, Faculty of Engineering, Gifu University, Gifu 501-1193, Japan*

Yuko Sugiyama − *Department of Chemistry and Biomolecular Science, Faculty of Engineering, Gifu University, Gifu 501-1193, Japan*

Complete contact information is available at: https://pubs.acs.org/10.1021/acsomega.1c02634

Notes

The authors declare no competing financial interest.

■ ACKNOWLEDGMENTS

This work was supported by JSPS KAKENHI (Scientific Research (C) 21K05098), Grant-in-Aid for Scientific Research on Innovative Areas from MEXT (15H00730), and Ogawa Science and Technology Foundation. Theoretical calculations were performed using the Research Center for Computational Science, Okazaki, Japan. This work was partly supported by Nanotechnology Platform Program (Molecule and Material Synthesis) (JPMXP09S20MS1032) of the Ministry of Education, Culture, Sports, Science and Technology (MEXT), Japan. The authors are thankful to Prof. Masahiro Ebihara for providing kind technical support.

■ REFERENCES

(1) Bera, J. K.; Dunbar, K. R. Chain Compounds Based on Transition Metal Backbones: New Life for an Old Topic. *Angew. Chem., Int. Ed.* **2002**, *41*, 4453−4457.

(2) Yamashita, M.; Takaishi, S. Tuning of Electronic Structures of Quasi-One-Dimensional Halogen-Bridged Ni-Pd Mixed-Metal Complexes, $[Ni_{1-x}Pd_x(chxn)_2X]X_2$ (X = Cl, Br) with Strong Electron Correlation. *Bull. Chem. Soc. Jpn.* **2006**, *79*, 1820−1833.

(3) Mashima, K. Linearly Aligned Metal Clusters: Versatile Reactivity and Bonding Nature of Tetrametal MMoMoM Complexes (M = Pt, Pd, Ir, and Rh) Supported by 6-Diphenylphosphino-2-pyridonato Ligand. *Bull. Chem. Soc. Jpn.* **2010**, *83*, 299−312.

(4) Beach, S. A.; Doerrer, L. H. Heterobimetallic Lantern Complexes and Their Novel Structural and Magnetic Properties. *Acc. Chem. Res.* **2018**, *51*, 1063−1072.

(5) Chipman, J. A.; Berry, J. F. Paramagnetic Metal−Metal Bonded Heterometallic Complexes. *Chem. Rev.* **2020**, *120*, 2409−2447.

(6) Campbell, M. G.; Powers, D. C.; Raynaud, J.; Graham, M. J.; Xie, P.; Lee, E.; Ritter, T. Synthesis and structure of solution-stable one-dimensional palladium wires. *Nat. Chem.* **2011**, *3*, 949−953.

(7) Givaja, G.; Amo-Ochoa, P.; Gómez-García, C. J.; Zamora, F. Electrical conductive coordination polymers. *Chem. Soc. Rev.* **2012**, *41*, 115−147.

(8) Chujo, Y.; Tanaka, K. New Polymeric Materials Based on Element-Blocks. *Bull. Chem. Soc. Jpn.* **2015**, *88*, 633−643.

(9) Wu, L.-P.; Field, P.; Morrissey, T.; Murphy, C.; Nagle, P.; Hathaway, B.; Simmons, C.; Thornton, P. Crystal Structure and Electronic Properties of Dibromo- and Dichloro-tetrakis[μ_3-bis(2-pyridyl)amido]triscopper(II) Hydrate. *J. Chem. Soc., Dalton Trans.* **1990**, 3835−3841.

(10) Shieh, S.-J.; Chou, C.-C.; Lee, G.-H.; Wang, C.-C.; Peng, S.-M. Linear Pentanuclear Complexes Containing a Chain of Metal Atoms: $[Co^{II}_5(\mu_5\text{-tpda})_4(NCS)_2]$ and $[Ni^{II}_5(\mu_5\text{-tpda})_4Cl_2]$. *Angew. Chem., Int. Ed.* **1997**, *36*, 56−59.

(11) Lai, S.-Y.; Lin, T.-W.; Chen, Y.-H.; Wang, C.-C.; Lee, G.-H.; Yang, M.-h.; Leung, M.-k.; Peng, S.-M. Metal String Complexes: Synthesis and Crystal Structure of $[Ni_4(\mu_4\text{-phdpda})_4]$ and $Ni_7(\mu_7\text{-teptra})_4Cl_2]$ (H_2phdpda = *N*-Phenyldipyridyldiamine and H_3teptra = Tetrapyridyltriamine). *J. Am. Chem. Soc.* **1999**, *121*, 250−251.

(12) Clérac, R.; Cotton, F. A.; Dunbar, K. R.; Lu, T.; Murillo, C. A.; Wang, X. A New Linear Tricobalt Compound with Di(2-pyridyl)amide (dpa) Ligands: Two-Step Spin Crossover of $[Co_3(dpa)_4Cl_2][BF_4]$. *J. Am. Chem. Soc.* **2000**, *122*, 2272−2278.

(13) Berry, J. F.; Cotton, F. A.; Lei, P.; Lu, T.; Murillo, C. A. Additional Steps toward Molecular Scale Wires: Further Study of $Ni_5^{10/11+}$ Chains Embranced by Polypyridylamide Ligands. *Inorg. Chem.* **2003**, *42*, 3534−3539.

(14) Ismayilov, R. H.; Wang, W.-Z.; Lee, G.-H.; Yeh, C.-Y.; Hua, S.-A.; Song, Y.; Rohmer, M.-M.; Bénard, M.; Peng, S.-M. Two Linear Undecanickel Mixed-Valence Complexes: Increasing the Size and the Scope of the Electronic Properties of Nickel Metal Strings. *Angew. Chem., Int. Ed.* **2011**, *50*, 2045−2048.
(15) Liu, I. P.-C.; Wang, W.-Z.; Peng, S.-M. New generation of metal string complexes: strengthening metal−metal interaction via naphthyridyl group modulated oligo-α-pyridylamido ligands. *Chem. Commun.* **2009**, 4323−4331.
(16) Nicolini, A.; Galavotti, R.; Barra, A.-L.; Borsari, M.; Caleffi, M.; Luo, G.; Novitchi, G.; Park, K.; Ranieri, A.; Rigamonti, L.; Roncaglia, F.; Train, C.; Cornia, A. Filling the Gap in Extended Metal Atom Chains: Ferromagnetic Interactions in a Tetrairon(II) String Supported by Oligo-α-pyridylamido Ligands. *Inorg. Chem.* **2018**, *57*, 5438−5448.
(17) Stollenz, M. Linear Copper Complex Arrays as Versatile Molecular Strings: Syntheses, Structures, Luminescence, and Magnetism. *Chem. - Eur. J.* **2019**, *25*, 4274−4298.
(18) Tanase, T.; Begum, R. A. Unsymmetrical A-Frame Pt_2Pd Trinuclear Complexes: Site-Selective Apparent Double Insertion of Alkynes into Pd-Pt and Pd-P Bonds. *Organometallics* **2001**, *20*, 106−114.
(19) Tanase, T.; Otaki, R.; Nishida, T.; Takenaka, H.; Takemura, Y.; Kure, B.; Nakajima, T.; Kitagawa, Y.; Tsubomura, T. Strongly Luminous Tetranuclear Gold(I) Complexes Supported by Tetraphosphine Ligands, *meso*- or *rac*-Bis[(diphenylphosphinomethyl)-phenylphosphino]methane. *Chem. - Eur. J.* **2014**, *20*, 1577−1596.
(20) Tanase, T.; Hatada, S.; Noda, S.; Takenaka, H.; Nakamae, K.; Kure, B.; Nakajima, T. Stepwise Expansion of Pd Chains from Binuclear Palladium(I) Complexes Supported by Tetraphosphine Ligands. *Inorg. Chem.* **2015**, *54*, 8298−8309.
(21) Nakajima, T.; Tanase, T. Transition Metal Clusters Constrained by Linear Tetradentate Phosphine Ligands. *Chem. Lett.* **2020**, *49*, 386−394.
(22) Murahashi, T.; Mochizuki, E.; Kai, Y.; Kurosawa, H. Organometallic Sandwich Chains Made of Conjugated Polyenes and Metal-Metal Chains. *J. Am. Chem. Soc.* **1999**, *121*, 10660−10661.
(23) Murahashi, T.; Uemura, T.; Kurosawa, H. Perylene-Tetrapalladium Sandwich Complexes. *J. Am. Chem. Soc.* **2003**, *125*, 8436−8437.
(24) Horiuchi, S.; Tachibana, Y.; Yamashita, M.; Yamamoto, K.; Masai, K.; Takase, K.; Matsutani, T.; Kawamata, S.; Kurashige, Y.; Yanai, T.; Murahashi, T. Multinuclear metal-binding ability of a carotene. *Nat. Commun.* **2015**, *6*, No. 6742.
(25) Hua, S.-A.; Cheng, M.-C.; Chen, C.-h.; Peng, S.-M. From Homonuclear Metal String Complexes to Heteronuclear Metal String Complexes. *Eur. J. Inorg. Chem.* **2015**, 2510−2523.
(26) Brogden, D. W.; Berry, J. F. Coordination Chemistry of 2,2′-Dipyridylamine: The Gift That Keeps on Giving. *Comments Inorg. Chem.* **2016**, *36*, 17−37.
(27) Nakano, H.; Nakamura, A.; Mashima, K. Linear Trinuclear Pt—Mo−Mo Complexes $[Mo_2PtX_2(pyphos)_2(O_2CR)_2]_2$ (X = Cl, Br, I; R = CH_3, $C(CH_3)_3$; pyphos = 6-(Diphenylphosphino)-2-pyridonate) with an Axial Interaction between the Quadruply Bonded Mo_2 Moiety and the Platinum Atom. *Inorg. Chem.* **1996**, *35*, 4007−4012.
(28) Rohmer, M.-M.; Liu, I. P.-C.; Lin, J.-C.; Chiu, M.-J.; Lee, C.-H.; Lee, G.-H.; Bénard, M.; López, X.; Peng, S.-M. Structural, Magnetic, and Theoretical Characterization of a Heterometallic Polypyridylamide Complex. *Angew. Chem., Int. Ed.* **2007**, *46*, 3533−3536.
(29) Nippe, M.; Berry, J. F. Introducing a Metal-Metal Multiply Bonded Group as an ″Axial Ligand″ to Iron: Synthetic Design of a Linear Cr−Cr—Fe Framework. *J. Am. Chem. Soc.* **2007**, *129*, 12684−12685.
(30) Huang, G.-C.; Bénard, M.; Rohmer, M.-M.; Li, L.-A.; Chiu, M.-J.; Yeh, C.-Y.; Lee, G.-H.; Peng, S.-M. $Ru_2M(dpa)_4Cl_2$ (M = Cu, Ni): Synthesis, Characterization, and Theoretical Analysis of Asymmetric Heterometal String Complexes of the Dipyridylamide Family. *Eur. J. Inorg. Chem.* **2008**, 1767−1777.
(31) Nippe, M.; Victor, E.; Berry, J. F. Do Metal−Metal Multiply-Bonded "Ligands" Have a *trans* Influence? Structural and Magnetic Comparisons of Heterometallic Cr≡Cr···Co and Mo≡Mo···Co Interactions. *Eur. J. Inorg. Chem.* **2008**, 5569−5572.
(32) Liu, I. P.-C.; Chen, C.-H.; Chen, C.-F.; Lee, G.-H.; Peng, S.-M. Asymmetric heterometal string complexes: stereochemical control of the unique isomer of (4,0)$[CuCuPd(npa)_4Cl][PF_6]$ and (4,0)-$[CuCuPt(npa)_4Cl][PF_6]$. *Chem. Commun.* **2009**, 577−579.
(33) Nippe, M.; Wang, J.; Bill, E.; Hope, H.; Dalal, N. S.; Berry, J. F. Crystals in Which Some Metal Atoms are More Equal Than Others: Inequalities From Crystal Packing and Their Spectroscopic/Magnetic Consequences. *J. Am. Chem. Soc.* **2010**, *132*, 14261−14272.
(34) Nippe, M.; Bill, E.; Berry, J. F. Group 6 Complexes with Iron and Zinc Heterometals: Understanding the Structural, Spectroscopic, and Electrochemical Properties of a Complete Series of M≡M—M′ Compounds. *Inorg. Chem.* **2011**, *50*, 7650−7661.
(35) Nippe, M.; Turov, Y.; Berry, J. F. Remote Effects of Axial Ligand Substitution in Heterometallic Cr≡Cr—M Chains. *Inorg. Chem.* **2011**, *50*, 10592−10599.
(36) Aydin-Cantürk, D.; Nuss, H. Synthesis, Structure Determination, and Magnetic Properties of the New Heterometallic Chain Compound $CrCrNi(di\text{-}2,2'\text{-}pyridylamido)_4Cl_2{\cdot}Et_2O$. *Z. Anorg. Allg. Chem.* **2011**, *637*, 543−546.
(37) Turov, Y.; Berry, J. F. Synthesis, characterization and thermal properties of trimetallic N_3−Cr≡Cr···M−N_3 azide complexes with M = Cr, Mn, Fe, and Co. *Dalton Trans.* **2012**, *41*, 8153−8161.
(38) Brogden, D. W.; Berry, J. F. Heterometallic Multiple Bonding: Delocalized Three-Center σ and π Bonding in Chains of 4d and 5d Transition Metals. *Inorg. Chem.* **2014**, *53*, 11354−11356.
(39) Brogden, D. W.; Berry, J. F. Heterometallic Second-Row Transition Metal Chain Compounds in Two Charge States: Syntheses, Properties, and Electronic Structures of $[Mo-Mo-Ru]^{6+/7+}$ Chains. *Inorg. Chem.* **2015**, *54*, 7660−7665.
(40) Brogden, D. W.; Christian, J. H.; Dalal, N. S.; Berry, J. F. Completing the series of Group VI heterotrimetallic $M_2Cr(dpa)_4Cl_2$ (M_2 = Cr_2, Mo_2, MoW and W_2) compounds and investigating their metal−metal interactions using density functional theory. *Inorg. Chim. Acta* **2015**, *424*, 241−247.
(41) Christian, J. H.; Brogden, D. W.; Bindra, J. K.; Kinyon, J. S.; Tol, J. V.; Wang, J.; Berry, J. F.; Dalal, N. S. Enhancing the Magnetic Anisotropy of Linear Cr(II) Chain Compounds Using Heavy Metal Substitutions. *Inorg. Chem.* **2016**, *55*, 6376−6383.
(42) Chipman, J. A.; Berry, J. F. Extraordinarily Large Ferromagnetic Coupling ($J \geq 150$ cm^{-1}) by Electron Delocalization in a Heterometallic Mo≡Mo−Ni Chain Complex. *Chem. - Eur. J.* **2018**, *24*, 1494−1499.
(43) Chipman, J. A.; Berry, J. F. Facile Axial Ligand Substitution in Linear Mo≡Mo−Ni Complexes. *Inorg. Chem.* **2018**, *57*, 9354−9363.
(44) Cheng, M.-C.; Hua, S.-A.; Lv, Q.; Sigrist, M.; Lee, G.-H.; Liu, Y.-C.; Chiang, M.-H.; Peng, S.-M. Stepwise synthesis of the heterotrimetallic chains $[MRu_2(dpa)_4X_2]^{0/1+}$ using group 7 to group 12 transition metal ions and $[Ru_2(dpa)_4Cl]$. *Dalton Trans.* **2018**, *47*, 1422−1434.
(45) Huang, M.-J.; Hua, S.-A.; Fu, M.-D.; Huang, G.-C.; Yin, C.; Ko, C.-H.; Kuo, C.-K.; Hsu, C.-H.; Lee, G.-H.; Ho, K.-Y.; Wang, C.-H.; Yang, Y.-W.; Chen, I.-C.; Peng, S.-M.; Chen, C.-h. The First Heteropentanuclear Extended Metal-Atom Chain: $[Ni^{+}-Ru_2^{5+}-Ni^{2+}-Ni^{2+}(tripyridyldiamido)_4(NCS)_2]$. *Chem. - Eur. J.* **2014**, *20*, 4526−4531.
(46) Chiu, C.-C.; Cheng, M.-C.; Lin, S.-H.; Yan, C.-W.; Lee, G.-H.; Chang, M.-C.; Lin, T.-S.; Peng, S.-M. Structure and magnetic properties of a novel heteroheptanuclear metal string complex $[Ni_3Ru_2Ni_2(\mu_7\text{-}teptra)_4(NCS)_2](PF_6)$. *Dalton Trans.* **2020**, *49*, 6635−6643.
(47) Nippe, M.; Timmer, G. H.; Berry, J. F. Remarkable regioselectivity in the preparation of the first heterotrimetallic Mo≡W—Cr chain. *Chem. Commun.* **2009**, 4357−4359.
(48) Cheng, M.-C.; Mai, C.-L.; Yeh, C.-Y.; Lee, G.-H.; Peng, S.-M. Facile synthesis of heterotrimetallic metal−string complex $[NiCoRh(dpa)_4Cl_2]$ through direct metal replacement. *Chem. Commun.* **2013**, *49*, 7938−7940.

https://doi.org/10.1021/acsomega.1c02634
ACS Omega 2021, 6, 18487−18503

(49) Cheng, M.-C.; Huang, R.-X.; Liu, Y.-C.; Chiang, M.-H.; Lee, G.-H.; Song, Y.; Lin, T.-S.; Peng, S.-M. Structures and paramagnetism of five heterometallic pentanuclear metal strings containing as many as four different metals: $NiPtCo_2Pd(tpda)_4Cl_2$. *Dalton Trans.* **2020**, *49*, 7299−7303.
(50) Uemura, K. One-dimensional complexes extended by unbridged metal−metal bonds based on a HOMO−LUMO interaction at the dz^2 orbital between platinum and heterometal atoms. *Dalton Trans.* **2017**, *46*, 5474−5492.
(51) Uemura, K.; Ebihara, M. One-Dimensionally Extended Paddlewheel Dirhodium Complexes from Metal−Metal Bonds with Diplatinum Complexes. *Inorg. Chem.* **2011**, *50*, 7919−7921.
(52) Uemura, K.; Kanbara, T.; Ebihara, M. Two Types of Heterometallic One-Dimensional Alignment Composed of Acetamidate-Bridged Dirhodium and Pivalamidate-Bridged Diplatinum Complexes. *Inorg. Chem.* **2014**, *53*, 4621−4628.
(53) Uemura, K.; Uesugi, N.; Matsuyama, A.; Ebihara, M.; Yoshikawa, H.; Awaga, K. Integration of Paramagnetic Diruthenium Complexes into an Extended Chain by Heterometallic Metal−Metal Bonds with Diplatinum Complexes. *Inorg. Chem.* **2016**, *55*, 7003−7011.
(54) Uemura, K.; Ito, D.; Pirillo, J.; Hijikata, Y.; Saeki, A. Modulation of Band Gaps toward Varying Conductivities in Heterometallic One-Dimensional Chains by Ligand Alteration and Third Metal Insertion. *ACS Omega* **2020**, *5*, 30502−30518.
(55) Uemura, K.; Ebihara, M. Paramagnetic One-Dimensional Chains Comprised of Trinuclear Pt−Cu−Pt and Paddlewheel Dirhodium Complexes with Metal−Metal Bonds. *Inorg. Chem.* **2013**, *52*, 5535−5550.
(56) Uemura, K.; Miyake, R. Paramagnetic One-Dimensional Chain Complex Consisting of Three Kinds of Metallic Species Showing Magnetic Interaction through Metal−Metal Bonds. *Inorg. Chem.* **2020**, *59*, 1692−1701.
(57) Uemura, K. Magnetic behavior in heterometallic one-dimensional chains or octanuclear complex regularly aligned with metal−metal bonds as −Rh−Rh−Pt−Cu−Pt. *J. Mol. Str.* **2018**, *1162*, 31−36.
(58) Uemura, K.; Sakurai, K.; Yasuda, E.; Ebihara, M. Crystal Structures and Adsorption Spectra of Mono-Dimensional Hexanuclear Heterometallic Complexes with No Bridge Assisted Rhodium−Platinum Bonds. *Polyhedron* **2012**, *45*, 35−42.
(59) Uemura, K.; Yamasaki, K.; Fukui, K.; Matsumoto, K. Synthesis of Amidate-hanging Platinum Mononuclear Complexes by Base Hydrolysis of Nitrile Complexes. *Inorg. Chim. Acta* **2007**, *360*, 2623−2630.
(60) Liu, F.; Chen, W. Oxidative Addition of Cl_2, HClO to Square-Planar Pt^{II} Complexes: Synthesis and Structural Characterization of Platinum(II) and Platinum(IV) Bis(amidate) Complexes. *Eur. J. Inorg. Chem.* **2006**, 1168−1173.
(61) Uemura, K.; Sugiyama, Y.; Yasuda, E.; Ebihara, M. Syntheses, crystal structures and copper-binding capabilities of amidate-hanging platinum mononuclear complexes containing alkylamine moieties. *Polyhedron* **2014**, *67*, 513−519.
(62) Cotton, F. A.; Murillo, C. A.; Walton, R. A. *Multiple Bonds Between Metal Atoms*, 3rd ed.; Springer Science and Business Media, Inc.: New York, 2005.
(63) Goto, E.; Begum, R. A.; Zhan, S.; Tanase, T.; Tanigaki, K.; Sakai, K. Linear, Redox-Active Pt_6 and $Pt_2Pd_2Pt_2$ Clusters. *Angew. Chem., Int. Ed.* **2004**, *43*, 5029−5032.
(64) Chien, C.-H.; Chang, J.-C.; Yeh, C.-Y.; Lee, G.-H.; Fang, J.-M.; Peng, S.-M. Novel linear hexanuclear cobalt string complexes (Co_6^{12+}) and one-electron reduction products (Co_6^{11+}) supported by four $bpyany^{2-}$ ligands. *Dalton Trans.* **2006**, 2106−2113.
(65) Chien, C.-H.; Chang, J.-C.; Yeh, C.-Y.; Lee, G.-H.; Fang, J.-M.; Song, Y.; Peng, S.-M. Weak antiferromagnetic coupling for novel linear hexanuclear nickel(II) string complexes (Ni_6^{12+}) and partial metal−metal bonds in their one-electron reduction products (Ni_6^{11+}). *Dalton Trans.* **2006**, 3249−3256.
(66) Tsao, T.-B.; Lo, S.-S.; Yeh, C.-Y.; Lee, G.-H.; Peng, S.-M. Novel multi-spin-state linear hexanickel complexes Ni_6^{11+} and their singly oxidized products Ni_6^{12+} with 1,8-naphthyridine-based ligands: Tuning the redox properties of the metal string. *Polyhedron* **2007**, *26*, 3833−3841.
(67) Liu, I. P.-C.; Chen, C.-F.; Hua, S.-A.; Chen, C.-H.; Wang, H.-T.; Lee, G.-H.; Peng, S.-M. Clear evidence of electron delocalization: synthesis, structure, magnetism, EPR and DFT calculation of the asymmetric hexanickel string complex containing a single mixed-valence $(Ni_2)^{3+}$ unit. *Dalton Trans.* **2009**, 3571−3573.
(68) Tanase, T.; Yamamoto, C.; Kure, B.; Nakajima, T. One-dimensional Anisotropic Metal-Organic Module Containing a Pt_6 Chain Terminated with Redox Active Ferrocenyl Units. *Chem. Lett.* **2014**, *43*, 913−915.
(69) Tejel, C.; Ciriano, M. A.; Villarroya, B. E.; Lopez, J. A.; Lahoz, F. J.; Oro, L. A. A Hexanuclear Iridium Chain. *Angew. Chem., Int. Ed.* **2003**, *42*, 529−532.
(70) Villarroya, B. E.; Tejel, C.; Rohmer, M.-M.; Oro, L. A.; Ciriano, M. A.; Bénard, M. Discrete Iridium Pyridonate Chains with Variable Metal Valence: Nature and Energetics of the Ir−Ir Bonding from DFT Calculations. *Inorg. Chem.* **2005**, *44*, 6536−6544.
(71) Kimizuka, N. Self-Assembly of Supramolecular Nanofibers. *Adv. Polym. Sci.* **2008**, *219*, 1−26.
(72) Jang, K.; Jung, G.; Nam, H. J.; Jung, D.-Y.; Son, S. U. One-Dimensional Organometallic Molecular Wires via Assembly of $Rh(CO)_2Cl$(amine): Chemical Control of Interchain Distances and Optical Properties. *J. Am. Chem. Soc.* **2009**, *131*, 12046−12047.
(73) Kuwahara, R.; Fujikawa, S.; Kuroiwa, K.; Kimizuka, N. Controlled Polymerization and Self-Assembly of Halogen-Bridged Diruthenium Complexes in Organic Media and Their Dielectrophoretic Alignment. *J. Am. Chem. Soc.* **2012**, *134*, 1192−1199.
(74) Jung, O.-S.; Kim, Y. J.; Lee, Y.-A.; Park, J. K.; Chae, H. K. Smart Molecular Helical Springs as Tunable Receptors. *J. Am. Chem. Soc.* **2000**, *122*, 9921−9925.
(75) Uemura, K.; Kumamoto, Y.; Kitagawa, S. Zipped-up Chain-type Coordination Polymers: Unsymmetrical Amide-containing Ligands Inducing β-Sheet or Helical Structures. *Chem. - Eur. J.* **2008**, *14*, 9565−9576.
(76) Das, K.; Kadish, K. M.; Bear, J. L. Substituent and Solvent Effects on the Electrochemical Properties of tetra-μ-carboxylato-dirhodium-(II). *Inorg. Chem.* **1978**, *17*, 930−934.
(77) Chavan, M. Y.; Zhu, T. P.; Lin, X. Q.; Ahsan, M. Q.; Bear, J. L.; Kadish, K. M. Axial-Ligand-Dependent Electrochemical and Spectral Properties of a Series of Acetate- and Acetamidate-Bridged Dirhodium Complexes. *Inorg. Chem.* **1984**, *23*, 4538−4545.
(78) Kawamura, T.; Katayama, H.; Nishikawa, H.; Yamabe, T. Ligand Dependence of Electronic Configuration of the Rh-Rh Bond in Rh_2^{5+} Complexes As Studied by Electron Spin Resonance and Electrochemistry. *J. Am. Chem. Soc.* **1989**, *111*, 8156−8160.
(79) Matsumoto, K.; Sakai, K. Structures and Reactivities of Platinum-Blues and the Related Amidate-bridged Platinum(III) Compounds. *Adv. Inorg. Chem.* **1999**, *49*, 375−427.
(80) Trasatti, S. The Absolute Electrode Potential: an Explanatory Note. *Pure Appl. Chem.* **1986**, *58*, 955−966.
(81) Pommerehne, J.; Vestweber, H.; Guss, W.; Mahrt, R. F.; Bässler, H.; Porsch, M.; Daub, J. Efficient Two Layer LEDs on a Polymer Blend Basis. *Adv. Mater.* **1995**, *7*, 551−554.
(82) Shafiee, A.; Salleh, M. M.; Yahaya, M. Determination of HOMO and LUMO of [6,6]-Phenyl C61-butyric Acid 3-ethylthiophene Ester and Poly (3-octyl-thiophene-2,5-diyl) through Voltametry Characterization. *Sains Malays.* **2011**, *40*, 173−176.
(83) Dhara, S. C. A Rapid Method for the Synthesis of *cis*-$[Pt(NH_3)_2Cl_2]$. *Indian J. Chem.* **1970**, 193−194.
(84) Rochon, F. D.; Buculei, V. Multinuclear NMR study and crystal structures of complexes of the types *cis*- and *trans*-Pt(amine)$_2I_2$. *Inorg. Chim. Acta* **2004**, *357*, 2218−2230.
(85) Rempel, G. A.; Legzdins, P.; Smith, H.; Wilkinson, G. Tetrakis(acetato)dirhodium(II) and Similar Carboxylato Compounds. *Inorg. Syn.* **1972**, *13*, 90−91.
(86) Lee, C. T.; Yang, W. T.; Parr, R. G. Development of the Colle-Salvetti correlation-energy formula into a functional of the electron density. *Phys. Rev. B* **1988**, *37*, 785−789.

https://doi.org/10.1021/acsomega.1c02634
ACS Omega 2021, 6, 18487−18503

(87) Miehlich, B.; Savin, A.; Stoll, H.; Preuss, H. Results obtained with the correlation energy density functionals of becke and Lee, Yang and Parr. *Chem. Phys. Lett.* **1989**, *157*, 200−206.
(88) Becke, A. D. Density-functional thermochemistry. III. The role of exact exchange. *J. Chem. Phys.* **1993**, *98*, 5648−5652.
(89) Frisch, M. J.; Trucks, G. W.; Schlegel, H. B.; Scuseria, G. E.; Robb, M. A.; Cheeseman, J. R.; Scalmani, G.; Barone, V.; Petersson, G. A.; Nakatsuji, H.; Li, X.; Caricato, M.; Marenich, A. V.; Bloino, J.; Janesko, B. G.; Gomperts, R.; Mennucci, B.; Hratchian, H. P.; Ortiz, J. V.; Izmaylov, A. F.; Sonnenberg, J. L.; Williams-Young, D.; Ding, F.; Lipparini, F.; Egidi, F.; Goings, J.; Peng, B.; Petrone, A.; Henderson, T.; Ranasinghe, D.; Zakrzewski, V. G.; Gao, J.; Rega, N.; Zheng, G.; Liang, W.; Hada, M.; Ehara, M.; Toyota, K.; Fukuda, R.; Hasegawa, J.; Ishida, M.; Nakajima, T.; Honda, Y.; Kitao, O.; Nakai, H.; Vreven, T.; Throssell, K.; Montgomery, J. A., Jr. *Gaussian 16*, revision C.01; Gaussian, Inc.: Wallingford, CT, 2016.
(90) Hay, P. J.; Wadt, W. R. Ab initio effective core potentials for molecular calculations. Potentials for K to Au including the outermost core orbitals. *J. Chem. Phys.* **1985**, *82*, 299−310.
(91) Hariharan, P. C.; Pople, J. A. The influence of polarization functions on molecular orbital hydrogenation energies. *Theor. Chim. Acta* **1973**, *28*, 213−222.
(92) Casida, M. E.; Jamorski, C.; Casida, K. C.; Salahub, D. R. Molecular excitation energies to high-lying bound states from time-dependent density-functional response theory: Characterization and correction of the time-dependent local density approximation ionization threshold. *J. Chem. Phys.* **1998**, *108*, 4439−4449.
(93) Stratmann, R. E.; Scuseria, G. E.; Frisch, M. J. An efficient implementation of time-dependent density-functional theory for the calculation of excitation energies of large molecules. *J. Chem. Phys.* **1998**, *109*, 8218−8224.
(94) *REQAB*, version 1.1; Rigaku Corp.: Tokyo, 1998.
(95) Altomare, A.; Burla, M. C.; Camalli, M.; Cascarano, G. L.; Giacovazzo, C.; Guagliardi, A.; Moliterni, A. G. G.; Polidori, G.; Spagna, R. SIR97: a new tool for crystal structure determination and refinement. *J. Appl. Crystallogr.* **1999**, *32*, 115−119.
(96) Sheldrick, G. M. A short history of SHELX. *Acta Crystallogr., Sect. A: Found. Crystallogr.* **2008**, *64*, 112−122.
(97) Kabuto, C.; Akine, S.; Nemoto, T.; Kwon, E. Release of software (Yadokari-XG 2009) for crystal structure analyses. *J. Crystallogr. Soc. Jpn.* **2009**, *51*, 218−224.

https://doi.org/10.1021/acsomega.1c02634
ACS Omega 2021, 6, 18487−18503